Engineering Structures 310 (2024) 118111

Contents lists available at ScienceDirect

Engineering Structures

journal homepage: www.elsevier.com/locate/engstruct

Dynamics of bridges during proof load tests and determination of mass-normalized mode shapes from OMA

Sandro Carbonari, Vanni Nicoletti *, Riccardo Martini, Fabrizio Gara

Dept. of Construction, Civil Engineering and Architecture (DICEA), Università Politecnica delle Marche, Ancona, Italy

ARTICLE INFO

Keywords:
Bridge-trucks dynamic coupling effect
Mass-normalized mode shapes
OMA on bridges
Stationed vehicles
Mass-change method
Bridge experimental modal identification
Parametric analyses

ABSTRACT

Modal shapes derived from Operational Modal Analysis (OMA) lack normalization with respect to masses, hindering direct estimation of effective mass or modal participation factors. The mass-change method is suitable to solve this issue since it proposes an experimental derivation of scaling factors for modes based on OMA results in different load conditions. However, in the case of bridges, the method application is challenging, as significant static masses are required on the deck for OMA in loaded conditions. To address this challenge, trucks can be used as added masses during standard static proof load tests for bridges, making the mass-change method feasible. However, the presence of trucks introduces dynamic coupling effects among bridge and vehicles, potentially complicating the dynamic identification. This paper proposes a methodology to exploit data obtained from OMA on bridges loaded with stationed trucks within the framework of the mass-change method in order to get the modal scaling factors for the mass normalisation of mode shapes and taking into account possible effects of the dynamic coupling between the two systems. To this purpose, the bridge dynamics with added stationed trucks is studied by introducing a finite element model to address the bridge-vehicles dynamic coupling. Then, a simple but effective 2-degree of freedom system is introduced to develop a parametric investigation in a non-dimensional manner in order to provide a practical tool for engineers to account for the bridge-truck dynamic coupling effects. Finally, numerical applications are proposed to derive some conclusions about the effectiveness of the proposed procedure and its suitability in real applications.

1. Introduction

Bridges play a primary role in the roadway and railway networks because any failure or service interruption cause significant direct and indirect losses. Consequently, design of bridges must be accurately performed, and their operational performance must be scrupulously checked [1,2]. Modal properties that characterize the dynamic behaviour of bridges may represent a useful support to achieve these targets because they can be used for the modelling check and validation, the response evaluation, quality control, assessment of real world structures, and health monitoring during the bridge life [3–5]. The main dynamic properties of interest are the resonance frequencies, modal damping, and mode shapes, as well as the Modal Participation Factor (MPF) and Modal Mass Ratio (MMR). MPF and MMR can be obtained from mass-normalized mode shapes [6], which are also useful for various applications, such as flexibility-based damage detection [7–9], identification of the physical stiffness, damping, and mass matrices of the system [10,11], and dynamic response reconstruction (e.g., frequency response functions and receptance matrix) [12,13].

The conventional experimental approach that allows for the identification of all the above quantities is based on the analysis of the vibration response due to a known excitation, which makes it possible to get the system Frequency Response Functions (FRFs). This process is known as input-output method, called Experimental Modal Analysis (EMA). However, for large-scale engineering structures such as bridges, the application of known forces becomes difficult and sometimes very expensive to do (if not impossible in many cases); so, the modal identification is performed through Ambient Vibration Tests (AVTs), considering the structural vibrations triggered by the so-called ambient noise, namely, vibrations produced by natural and anthropic sources of excitation; this approach is known as output-only method, called Operational Modal Analysis (OMA). However, OMA presents some drawbacks, such as the impossibility to measure the ambient noise, hence to get the mass-normalised modes, which are needed to determine the MPF and the MMR of vibration modes.

Besides some methods using the deflection under static loads in

* Corresponding author.
E-mail address: v.nicoletti@univpm.it (V. Nicoletti).

https://doi.org/10.1016/j.engstruct.2024.118111
Received 23 December 2023; Received in revised form 9 April 2024; Accepted 24 April 2024
Available online 4 May 2024

conjunction with model parameters from OMA are available in the literature (e.g. [14]), the most adopted approach is the mass-change method. The concept of this method is rather simple and based on the assumption that a controlled increment of masses on the structure does not produce a substantial change in the mode shapes. Thus, by adding one or more known masses to the tested structure, the experimental mode shapes can be mass-normalized by means of the measured shift in natural frequencies between the original and mass-loaded condition. Hence, the method is based on the sensitivity of modal parameters to changes in the structure's mass.

Several works in the literature deal with the topic of mode scaling from OMA results by adopting the mass-change method. Brincker and Andersen [15] were the first to propose a mass-change method application and a scaling factor estimation formula. Bernal [16] and Coppotelli [17] used the mass-change method to identify scaled mode shapes for the estimation of the FRFs. Lopez-Aenlle et al. [18] proposed a procedure to optimize the mass-change strategy based on modal parameters of the original (unloaded) structure, also discussing about the uncertainty on the scaling factor estimation depending on the modal analysis accuracy and the mass-change strategy, i.e., number, magnitude, and location of masses. Other researchers tried to improve the mass-change method considering low sensor count equipment [19], low frequency content [20], and incomplete measurement from OMA [21]. An alternative to the mass-change method consists of changing the stiffness of the structure (stiffness-change method) [22,23]. Nevertheless, this methodology is less adopted in real civil engineering structures due to easily understandable practical difficulties. Indeed, changes in bridge stiffness could be due to different factors, such as the presence of damage, variation of boundary conditions, and changes in environmental parameters.

At the beginning, the mass-change method was mainly applied and tested on simple mechanical systems. To the author's best knowledge, first applications on civil engineering structures are quite recent and dates back to 2005. Parloo et al. [24] in a first work proposed a mass-change method for scaling mode shapes; then, in a following research [25], they applied this method to a bridge case study: the bridge was loaded by six 1 m^3-concrete blocks to obtain the mass-loaded configuration, and the blocks were distributed all along the bridge deck. However, the application of concrete blocks is quite impractical because of issues related to long-term bridge shutdown and the use of expensive equipment and procedures for tests. For these reasons, recent works consider vehicles over the bridge as added masses. He et al. [26] developed a method based on a parked vehicle for mass perturbation and a moving vehicle for data collection, while Tian et al. [27] used only moving vehicles as added masses. Sheibani et al. [28] used the masses of moving vehicles over the bridge to induce the required mass modifications: motorway bridges under ambient forces or light traffic movement were considered as the original structure (unloaded), and an OMA test was conducted. Additionally, the bridge was tested again under heavily congested traffic movement, and this was regarded as the perturbed state (loaded condition). Furthermore, in a more recent work [29], this method was improved and extended to real traffic situation since the traffic load is not constant over time (sensitivity analysis regarding the uncertainty of the traffic loads were performed). However, all the above studies neglect the effects of the dynamic coupling between the bridge and vehicles, assuming the latter to contribute only in terms of mass.

The great advantage in using the mass-change method for obtaining scaled mode shapes resides in its simplicity and in the fact that only mode shapes and natural frequencies have to be determined, in addition to the added masses that must be known. However, the use of vehicles as added masses leads to the development of dynamic coupling effects between the two systems (vehicles and bridge). Indeed, vehicles are characterised not only by a proper mass, but also by stiffness properties, mainly due to the properties of tyres and the suspension system; thus, vehicles could be defined as "flexible" masses. Fortunately, if stationed vehicles are taken into account, dynamic effects due to the vehicles movement are absent. Hence, it can be asserted that the mass-change method can be used exploiting stationed vehicles, provided that the bridge-vehicles dynamic coupling effects triggered by the mass compliance is suitably taken into account.

In the literature, there are many studies that analyse the dynamic interaction phenomena between moving vehicles and bridges [30–32]; however, these works are mainly focused on understanding how a vehicle that is moving on the bridge deck can influence its dynamic response, also leading to possible and dangerous global and local resonance phenomena. In this field, it is common to refer to bridge-vehicle interaction phenomena. On the contrary, only few works are available in the literature discussing the dynamic coupling effects occurring when vehicles (e.g., trucks) are stationed over the deck [33–35], which is the main issue to address in order to extend the mass-change method to the use of stationed vehicles. The latter topic, differently from the former, is mainly focused on aspects relevant to the modal identification of bridges and it is addressed in this work.

In this work, a methodology to exploit data obtained from OMA on bridges loaded with stationed trucks within the framework of the mass-change method is presented in order to get the modal scaling factors for the mass normalisation of modes. The original idea of this work resides in taking into account the dynamic coupling effects arising when trucks are stationary placed on a bridge deck in the evaluation of the frequency shift to be used in the mass-change method. Trucks of known weight are always available when standard loading proof tests are performed for new bridges, which are mandatory before the opening to traffic, and the mass mobility makes it possible to perform AVTs considering suitable truck layouts. In addition, the use of trucks as added mass makes the proposed methodology also feasible in case of existing bridges, when their assessment needs to be carried out.

At the beginning of the paper, a brief recall of the mass-change method basics is proposed. Then, a Finite Element (FE) model is presented to investigate the topic of the dynamic coupling between bridge and stationed trucks, discussing some typical issues on the dynamic identification of bridges loaded by trucks. Then, a simpler but still effective analytical model is presented and validated through the comparison with the FE model results. The simple model is an evolution of the one proposed by Chang et al. [35] and it has been formulated in a non-dimensional form with the aim of providing a tool of general and large validity to be used in the majority of real applications to correctly determine the frequency shift to be used in the mass-change method. In order to provide the above tool, a non-dimensional parametric analysis is performed, based on the simple model, taking the opportunity to investigate which parameters mostly affect the dynamic coupling effects between the two systems (bridge and stationed trucks) when common loading proof tests are executed. Finally, an illustrative example of the proposed method is reported with general suggestions for real applications, in terms of truck layout and weight, in order to obtain effective mode scaling factors.

2. Brief recall of the mass-change method basics

The framework for obtaining mode scale factors from OMA adopting the mass-change method is rather simple and can be summarized in the following steps: (*i*) OMA is performed on the original structure (generally unloaded), (*ii*) the structural characteristics are modified by adding additional masses, (*iii*) OMA is repeated on the mass-loaded structure, (*iv*) the mode shape scaling factors are determined.

Several approaches and strategies have been studied in the literature for the determination of the scaling factors; a comprehensive study about this topic can be found in [22]. In this work, the simple formula proposed by Aenlle-Lopez et al. [18] is adopted, which can be derived from the eigenvalue problem of the original and the modified structures. For real-life engineering structures (such as bridges) with a predominant linear behaviour and low damping ratios (as commonly expected for ambient vibration excitations), the eigenvalue problem for the unloaded system can be written in the form:

$$(\mathbf{K}_0 - \omega_0^2 \mathbf{M}_0)\boldsymbol{\psi}_0 = \boldsymbol{0} \tag{1}$$

where $\mathbf{K}_0$ and $\mathbf{M}_0$ are the stiffness and mass matrices of the unloaded system, respectively, ω_0 is the circular frequency, and $\boldsymbol{\psi}_0$ is the mode shape vector. If a mass change is applied to the structure, the eigenvalue problem relevant to the loaded system becomes:

$$\left[\mathbf{K}_0 - \omega_1^2(\mathbf{M}_0 + \Delta\mathbf{M})\right]\boldsymbol{\psi}_1 = \boldsymbol{0} \tag{2}$$

where $\mathbf{M}_0 + \Delta\mathbf{M}$ is the new mass matrix, $\Delta\mathbf{M}$ is the matrix of the added masses, ω_1 is the circular frequency of the loaded system, and $\boldsymbol{\psi}_1$ is the mode shape vector of the loaded structure. By subtracting Eq. 2 from Eq. 1 the following expression is obtained:

$$\mathbf{M}_0\left(\omega_0^2\boldsymbol{\psi}_0 - \omega_1^2\boldsymbol{\psi}_1\right) - \omega_1^2\Delta\mathbf{M}\boldsymbol{\psi}_1 = \mathbf{K}_0(\boldsymbol{\psi}_0 - \boldsymbol{\psi}_1) \tag{3}$$

Assuming that the mass change is such that the mode shapes do not significantly change (i.e., $\boldsymbol{\psi}_1 \cong \boldsymbol{\psi}_0 \cong \boldsymbol{\psi}$), and pre-multiplying Eq. 3 by $\boldsymbol{\psi}^T$, the following equation is obtained:

$$\boldsymbol{\psi}^T\mathbf{M}_0\boldsymbol{\psi}\left(\omega_0^2 - \omega_1^2\right) - \omega_1^2\boldsymbol{\psi}^T\Delta\mathbf{M}\boldsymbol{\psi} = \mathbf{0} \tag{4}$$

Taking into account the orthogonality condition $\boldsymbol{\psi}^T\mathbf{M}\boldsymbol{\psi} = 1$, and considering that the relationship between the unscaled mode shape vector $\boldsymbol{\phi}$ (e.g., obtained from OMA) and the corresponding correctly scaled mode shape vector $\boldsymbol{\psi}$ can be expressed by:

$$\boldsymbol{\psi} = \alpha\boldsymbol{\phi} \tag{5}$$

Eq. 4 leads to obtain the scaling factor α:

$$\alpha = \sqrt{\frac{(\omega_0^2 - \omega_1^2)}{\omega_1^2\boldsymbol{\phi}^T\Delta\mathbf{M}\boldsymbol{\phi}}} \tag{6}$$

The mode shape can be obtained starting from both the loaded ($\boldsymbol{\phi}_1$) or unloaded ($\boldsymbol{\phi}_0$) structure, even if the one from the unloaded structure is commonly used.

In order to produce accurate and reliable normalization results some recommendations should be followed:

- added masses should be suitably distributed and not too large, in order to avoid significant variations of the mode shape [15]. A reasonable mass change entity is suggested around 5-10% of the total mass of the structure in [36]. However, the shift in natural frequency between the loaded and unloaded conditions should be large enough to allow for an accurate identification [22] beyond uncertainties due to identification methods;
- additional masses should not be placed in or near to nodal points of the mode shape considered for the normalization [25];
- mass changing in multiple locations is preferred [25]. A number of masses equal to or greater than the number of sagging and hogging regions of the mode shape is sufficient for each mode [18].

Overall, it can be concluded that the mass change must be high enough to maximize the frequency shift but, on the other hand, limited to minimize changes in mode shapes. For this reason, a rational recommendation is that of distributing as much as possible the added masses in order to limit the mode shape variation. However, standard recommendations for bridges are not available in the literature yet since they strongly depend on the structural typology. In the field of bridges, a contribution is provided in this sense in the present work with reference to a simply supported deck. However, further applications of this methodology on real structures are encouraged to define more detailed strategies in this regard.

3. Definition of a finite element model for the numerical investigation of bridge-vehicles dynamic coupling effects

During a bridge proof load test, trucks are usually stationed over the deck in different positions with the aim of producing severe load conditions for the structure and maximizing sagging and hogging bending moments in critical cross-sections. Also, when trucks are stationed over a bridge deck, the two systems (bridge and trucks) are not dynamically independent, but they interact each other; so, the resonance frequencies of the coupled system depend on different parameters, such as the stiffness and mass ratios between the two dynamic systems.

In this Section, a FE model is developed for investigating the above mentioned dynamic coupling effects. The FE is based on the coupling of a beam element of length L with a concentrated spring-mass system at one edge (Fig. 1**a**); damping is not included because the problem of the free undamped vibration is addressed. The dynamic problem is formulated in the frequency domain, so that forces and displacements reported below are implicitly assumed to be the Fourier Transforms of the corresponding quantities expressed in the time domain.

A frame reference system 0: x, y, z is introduced, with axis z oriented along the beam longitudinal direction, and the following displacement vector is considered:

$$\mathbf{u}(\omega, z) = \left[u_y(\omega, z) \quad u_z(\omega, z)\right]^T \tag{7}$$

collecting the beam displacement components along the y and z axes as a function of time. Similarly, the relative displacement of the concentrated masses with respect to the beam edge are collected in the following vector:

$$\mathbf{v}(\omega) = \left[v_y(\omega) \quad v_z(\omega)\right]^T \tag{8}$$

According to the Euler-Bernulli beam model, the following differential operator is introduced for evaluating the beam curvature and axial strain starting from displacements:

$$\mathscr{D}\mathbf{u}(\omega, z) = \left[-\frac{\partial^2 u_y}{\partial z^2} \quad \frac{\partial u_z}{\partial z}\right]^T \tag{9}$$

The beam has distributed masses deriving from the self-weight and additional masses coming from loads and non-structural elements of the bridge. By defining with ρ the material density and with A the cross-section area of the beam, the following mass matrix can be assembled:

$$\mathbf{M} = \rho A\begin{bmatrix}1 & 0\\0 & 1\end{bmatrix} + \begin{bmatrix}m_{d,v} & 0\\0 & m_{d,h}\end{bmatrix} \tag{10}$$

where $m_{d,v}$ and $m_{d,h}$ are the added distributed mass of the deck in the vertical and horizontal directions, respectively. Taking into account Eq. 9, the beam stresses are expressed by the following equation under the assumption of linear elastic material:

$$\mathbf{s}(\omega, z) = \mathbf{K}\mathscr{D}\mathbf{u}(\omega, z) \tag{11}$$

where

$$\mathbf{K}(z) = E\begin{bmatrix}I(z) & 0\\0 & A(z)\end{bmatrix} \tag{12}$$

is the cross-section stiffness matrix of the beam. In Eq. 12, E and I are the Young's modulus of the beam material and the inertia of the beam cross-section, respectively, which may change along the beam axis.

The stiffness and mass matrices of the lumped spring-mass system at the beam edge are similarly defined according to Eq. 13:

$$\bar{\mathbf{K}} = \begin{bmatrix}k_v & 0\\0 & k_h\end{bmatrix}; \quad \bar{\mathbf{M}} = \begin{bmatrix}m_v & 0\\0 & m_h\end{bmatrix} \tag{13}$$

where k_v and k_h are the vertical and horizontal stiffness of the lumped spring, respectively, and m_v and m_h are the lumped vertical and hori-

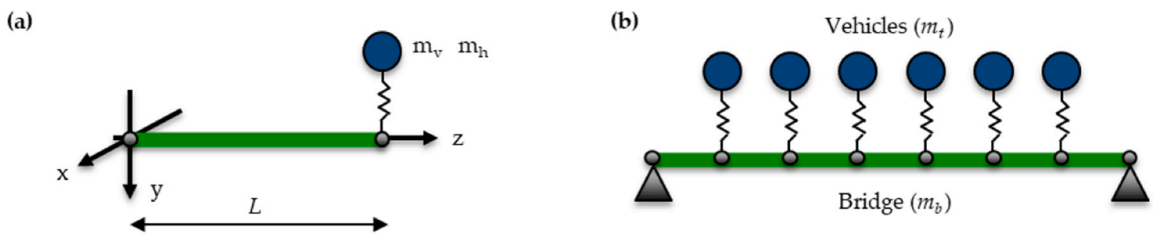

Fig. 1. Schematization of the proposed FE model: (a) single FE component, (b) model of the loaded bridge.

zontal masses representative of the single truck. The equilibrium condition for the undamped free vibration of the coupled beam-lumped system can be written in weak form by the Lagrange D′Alembert principle by assuming that the work resulting from inertia forces acting through every virtual consistent displacement field $\hat{\mathbf{u}}(z)$ and $\hat{\mathbf{v}}$ is equal to that resulting from stresses, acting through every virtual strain field $\mathscr{D}\hat{\mathbf{u}}(z)$, and bridge-truck interacting forces, acting through every virtual consistent displacement field $\hat{\mathbf{u}}(z)$ and $\hat{\mathbf{v}}$. In the frequency domain, this provides the following equation:

$$\begin{aligned}&\int_0^L \mathbf{K}\mathscr{D}\mathbf{u}(\omega,z)\cdot\mathscr{D}\hat{\mathbf{u}}(z)dz-\omega^2\int_0^L \mathbf{M}\mathbf{u}(\omega,z)\cdot\hat{\mathbf{u}}(z)dz-\bar{\mathbf{K}}\mathbf{v}(\omega)\cdot\hat{\mathbf{u}}(L)\\&+\bar{\mathbf{K}}\mathbf{v}(\omega)\cdot\hat{\mathbf{v}}-\omega^2\bar{\mathbf{M}}[\mathbf{v}(\omega)+\mathbf{u}(L,\omega)]\cdot\hat{\mathbf{v}}\\&=0\ \forall\hat{\mathbf{u}}(z)\neq\mathbf{0}\ \ \forall\hat{\mathbf{v}}\neq\mathbf{0}\end{aligned}\tag{14}$$

with the relevant boundary conditions:

$$\mathbf{u}(\omega,0)=\mathbf{u}_0(\omega);\quad \mathbf{u}(\omega,L)=\mathbf{u}_L(\omega);\quad \mathbf{v}(\omega)=\mathbf{v}_0(\omega)\tag{15}$$

With the purpose of exploiting the above equation for the definition of a FE, the following vector $\mathbf{d}(\omega,z)$ is defined, collecting the beam displacements and those of the spring-mass system:

$$\mathbf{d}(\omega,z)=\begin{bmatrix}\mathbf{u}(\omega,z)\\ \mathbf{v}(\omega)\end{bmatrix}\tag{16}$$

Sub-vectors $\mathbf{u}(\omega,z)$ and $\mathbf{v}(\omega)$ can be obtained from Eq. 16 through equations:

$$\mathbf{u}=\mathbf{a}_u\mathbf{d};\qquad \mathbf{v}=\mathbf{a}_v\mathbf{d}\tag{17}$$

where

$$\mathbf{a}_u=[\mathbf{1}\quad\mathbf{0}];\quad \mathbf{a}_v=[\mathbf{0}\quad\mathbf{1}]\tag{18}$$

are geometric operators in which $\mathbf{1}$ is the identity matrix of order 2 and $\mathbf{0}$ is a null matrix of order 2. Taking into account Eq. 17, Eq. 14 yields:

$$\begin{aligned}&\int_0^L \mathbf{K}\mathbf{a}_u\mathscr{D}\mathbf{d}(\omega,z)\cdot\mathbf{a}_u\mathscr{D}\hat{\mathbf{d}}(z)dz-\omega^2\int_0^L \mathbf{M}\mathbf{a}_u\mathbf{d}(\omega,z)\cdot\mathbf{a}_u\hat{\mathbf{d}}(z)dz\\&-\bar{\mathbf{K}}\mathbf{a}_v\mathbf{d}(\omega,z)\cdot\mathbf{a}_u\hat{\mathbf{d}}(z)+\left(\bar{\mathbf{K}}-\omega^2\bar{\mathbf{M}}\right)\mathbf{a}_v\mathbf{d}(\omega,z)\cdot\mathbf{a}_v\hat{\mathbf{d}}(z)\\&-\omega^2\bar{\mathbf{M}}\mathbf{a}_u\mathbf{d}(\omega,z)\cdot\mathbf{a}_v\hat{\mathbf{d}}(z)\\&=0\quad\forall\hat{\mathbf{d}}\neq\mathbf{0}\end{aligned}\tag{19}$$

with the relevant boundary conditions

$$\mathbf{d}(\omega,0)=\mathbf{d}_0(\omega);\quad \mathbf{d}(\omega,L)=\mathbf{d}_L(\omega)\tag{20}$$

In the displacement based approach, the solution of Eq. 19 is obtained numerically by the FE method considering the third order polynomials for the vertical displacements and first order polynomials for the axial ones to obtain an interdependent interpolation element. Three degrees of freedom are associated to each node of the FE, namely two translations and a rotation, so that the complete vector of the FE displacements is constituted by eight components, in order to include the vertical and horizontal displacements of the lumped mass at the element edge. Displacement components of the FE with generic nodes i and j are collected in vector:

$$\mathbf{d}^e(\omega)=[u_{yi}\quad u_{zi}\quad \varphi_{xi}\quad u_{yj}\quad u_{zj}\quad \varphi_{xj}\quad v_y\quad v_z]^T\tag{21}$$

The displacements within the element may be expressed as:

$$\mathbf{d}(\omega,z)\cong\mathbf{N}^e(z)\mathbf{d}^e(\omega)\tag{22}$$

where:

$$\mathbf{N}^e=\begin{bmatrix}\mathbf{N}^b & \mathbf{0}\\ \mathbf{0} & \mathbf{I}_{2x2}\end{bmatrix}=\begin{bmatrix}n_1(z) & 0 & -n_2(z) & n_3(z) & 0 & -n_4(z) & 0 & 0\\ 0 & n_5(z) & 0 & 0 & n_6(z) & 0 & 0 & 0\\ 0 & 0 & 0 & 0 & 0 & 0 & 1 & 0\\ 0 & 0 & 0 & 0 & 0 & 0 & 0 & 1\end{bmatrix}\tag{23}$$

is the matrix of the interpolating polynomials. By considering the approximation of Eq. 22, the balance condition of Eq. 19 becomes:

$$\begin{aligned}&\int_0^L(\mathscr{D}\mathbf{N}^e)^T\mathbf{a}_u^T\mathbf{K}\mathbf{a}_u(\mathscr{D}\mathbf{N}^e)\mathbf{d}^e\cdot\hat{\mathbf{d}}^e dz-\omega^2\int_0^L(\mathbf{N}^e)^T\mathbf{a}_u^T\mathbf{M}\mathbf{a}_u\mathbf{N}^e\mathbf{d}^e\cdot\hat{\mathbf{d}}^e dz\\&-(\mathbf{N}^e(z))^T\mathbf{a}_u^T\bar{\mathbf{K}}\mathbf{a}_v\mathbf{N}^e(z)\mathbf{d}^e(\omega)\cdot\hat{\mathbf{d}}^e+(\mathbf{N}^e)^T\mathbf{a}_v^T\left(\bar{\mathbf{K}}-\omega^2\bar{\mathbf{M}}\right)\mathbf{a}_v\mathbf{N}^e\mathbf{d}^e\cdot\hat{\mathbf{d}}^e\\&-\omega^2(\mathbf{N}^e)^T\mathbf{a}_v^T\bar{\mathbf{M}}\mathbf{a}_u\mathbf{N}^e\mathbf{d}^e\cdot\hat{\mathbf{d}}^e\\&=0\quad\forall\hat{\mathbf{d}}^e\neq\mathbf{0}\end{aligned}\tag{24}$$

with the relevant boundary conditions imposed on one side of the element or at the lumped masses. In Eq. 24 the terms

$$\begin{aligned}\mathbf{K}_e=&\int_0^L(\mathscr{D}\mathbf{N}^e)^T\mathbf{a}_u^T\mathbf{K}\mathbf{a}_u(\mathscr{D}\mathbf{N}^e)\mathbf{d}^e dz-(\mathbf{N}^e(z))^T\mathbf{a}_u^T\bar{\mathbf{K}}\mathbf{a}_v\mathbf{N}^e(z)\mathbf{d}^e(\omega)\\&+(\mathbf{N}^e)^T\mathbf{a}_v^T\bar{\mathbf{K}}\mathbf{a}_v\mathbf{N}^e\mathbf{d}^e\end{aligned}\tag{25a}$$

$$\mathbf{M}_e=\int_0^L(\mathbf{N}^e)^T\mathbf{a}_u^T\mathbf{M}\mathbf{a}_u\mathbf{N}^e\mathbf{d}^e dz+(\mathbf{N}^e)^T\mathbf{a}_v^T(\bar{\mathbf{M}})\mathbf{a}_v\mathbf{N}^e\mathbf{d}^e+(\mathbf{N}^e)^T\mathbf{a}_v^T\bar{\mathbf{M}}\mathbf{a}_u\mathbf{N}^e\mathbf{d}^e\tag{25b}$$

are the stiffness and mass matrices of the proposed FE. Thus, the balance condition of Eq. 24 can be simplified into the following equation:

$$\left(\mathbf{K}_e-\omega^2\mathbf{M}_e\right)\mathbf{d}^e(\omega)=\mathbf{0}\tag{26}$$

By partitioning vector $\mathbf{d}^e$ as follows:

$$\mathbf{d}=\begin{bmatrix}\mathbf{d}_i^e(\omega)\\ \mathbf{d}_j^e(\omega)\\ \mathbf{v}(\omega)\end{bmatrix}\tag{27}$$

to highlight displacements of nodes i and j of the FE and of the lumped masses, the following expressions can be obtained for the stiffness and mass matrices of the FE:

$$\mathbf{K}_e=\begin{bmatrix}\mathbf{K}_{ii}^e & \mathbf{K}_{ij}^e & \mathbf{0}\\ \mathbf{K}_{ij}^e & \mathbf{K}_{jj}^e & -\bar{\mathbf{K}}\\ \mathbf{0} & \mathbf{0} & \bar{\mathbf{K}}\end{bmatrix};\quad \mathbf{M}_e=\begin{bmatrix}\mathbf{M}_{ii}^e & \mathbf{M}_{ij}^e & \mathbf{0}\\ \mathbf{M}_{ij}^e & \mathbf{M}_{jj}^e & \mathbf{0}\\ \mathbf{0} & \bar{\mathbf{M}} & \bar{\mathbf{M}}\end{bmatrix}\tag{28}$$

Eq. 28 can be assembled in the spirit of the FE approach to model different situations. For example, in case of single span bridge with a truck positioned at midspan, two FE can be assembled and the lumped masses of the second element can be made zero. Obviously, also non-symmetrical load conditions can be simulated by simply dividing the span into a suitable number of finite elements and neglecting the additional mass in those elements where trucks are not present. The same approach can be adopted in case a refined mesh is needed. The approach requires that at each truck position a node of the FE grid is available and that lumped springs are always greater than 0 (including cases in which masses are set to 0) in order to avoid numerical problems. In assembling the discrete problem, it is convenient, although not mandatory, to suitably arrange the displacement vector in order to separate displacements of the FE grid belonging to the beam from the displacement of the added masses (representative of the trucks). Once the problem is assembled, boundary conditions are imposed in terms of imposed displacements (e.g., homogenous boundary conditions, corresponding to external restrains, or non-homogenous boundary conditions). If homogeneous boundary conditions are applied, the following system of equations can be obtained, by suitably partitioning free (f) and restrained (r) nodes:

$$\left(\begin{bmatrix}\mathbf{K}_{e,ff} & \mathbf{K}_{e,fr}\\ \mathbf{K}_{e,rf} & \mathbf{K}_{e,rr}\end{bmatrix} - \omega^2\begin{bmatrix}\mathbf{M}_{e,ff} & \mathbf{M}_{e,fr}\\ \mathbf{M}_{e,rf} & \mathbf{M}_{e,rr}\end{bmatrix}\right)\begin{bmatrix}\mathbf{d}^{e,ff}(\boldsymbol{\omega})\\ \mathbf{0}\end{bmatrix} = \mathbf{0} \tag{29}$$

from which the following eigenvalue problem can be extracted and solved to get the fundamental resonance frequencies and mode shapes of the system:

$$\left(\mathbf{K}_{e,ff} - \omega^2\mathbf{M}_{e,ff}\right)\mathbf{d}^{e,ff}(\omega) = \mathbf{0} \tag{30}$$

If non-homogeneous boundary conditions are applied, or external forces are considered, the problem solution requires the definition of a source of damping in order to avoid resonance problems. In this case, viscous damping can be introduced according to the Rayleight method or hysteretic damping can be considered by introducing a complex-valued stiffness matrix. Thus, Eq. 29 transforms into:

$$\left(\begin{bmatrix}\mathbf{K}_{e,ff} & \mathbf{K}_{e,fr}\\ \mathbf{K}_{e,rf} & \mathbf{K}_{e,rr}\end{bmatrix} - \omega^2\begin{bmatrix}\mathbf{M}_{e,ff} & \mathbf{M}_{e,fr}\\ \mathbf{M}_{e,rf} & \mathbf{M}_{e,rr}\end{bmatrix} + i\omega\begin{bmatrix}\mathbf{C}_{e,ff} & \mathbf{C}_{e,fr}\\ \mathbf{C}_{e,rf} & \mathbf{C}_{e,rr}\end{bmatrix}\right)\begin{bmatrix}\mathbf{d}^{e,ff}(\boldsymbol{\omega})\\ \mathbf{d}^{e,rr}(\boldsymbol{\omega})\end{bmatrix} = \begin{bmatrix}\mathbf{f}^{e,ff}(\boldsymbol{\omega})\\ \mathbf{f}^{e,rr}(\boldsymbol{\omega})\end{bmatrix} \tag{31}$$

where $\mathbf{d}^{e,rr}(\boldsymbol{\omega})$ are the known imposed displacements, $\mathbf{f}^{e,ff}(\omega)$ are the known imposed forces at the free nodes of the system, while $\mathbf{d}^{e,ff}(\omega)$ are the unknown displacements of the free nodes and $\mathbf{f}^{e,rr}(\omega)$ are the unknown base reactions. In Eq. 31 the damping matrix $\mathbf{C}$ can assume the following expressions for the viscous and hysteretic damping, respectively:

$$\begin{bmatrix}\mathbf{C}_{e,ff} & \mathbf{C}_{e,fr}\\ \mathbf{C}_{e,rf} & \mathbf{C}_{e,rr}\end{bmatrix} = \beta\begin{bmatrix}\mathbf{M}_{e,ff} & \mathbf{M}_{e,fr}\\ \mathbf{M}_{e,rf} & \mathbf{M}_{e,rr}\end{bmatrix} + \delta\begin{bmatrix}\mathbf{K}_{e,ff} & \mathbf{K}_{e,fr}\\ \mathbf{K}_{e,rf} & \mathbf{K}_{e,rr}\end{bmatrix} \tag{32a}$$

$$\begin{bmatrix}\mathbf{C}_{e,ff} & \mathbf{C}_{e,fr}\\ \mathbf{C}_{e,rf} & \mathbf{C}_{e,rr}\end{bmatrix} = \frac{2\xi}{\omega}\begin{bmatrix}\mathbf{K}_{e,ff} & \mathbf{K}_{e,fr}\\ \mathbf{K}_{e,rf} & \mathbf{K}_{e,rr}\end{bmatrix} \tag{32b}$$

where β and δ are the well-known Rayleight coefficients and ξ is the desired damping ratio of the system.

The dynamic coupling effect between bridge and stationed vehicles is studied starting from the discussed FE model, and considering the configuration reported in Fig. 1**b**, where vehicles are supposed to be identical and uniformly distributed along the span length. Considering these hypotheses, the system is characterized by masses m_t and m_b, which represent the overall bridge and truck masses, respectively, by the overall vertical stiffness of trucks (due to tires and shock absorbers), and by the flexural stiffness of the bridge; above quantities define the resonance frequency of the unloaded bridge (ω_b) and of trucks (ω_t) when systems are decoupled. The resonance frequencies of the coupled system are obtained through a conventional eigenvalue analysis neglecting damping; this approach is reasonable considering that damping arising from very low excitations (e.g., ambient noise provided by micro-tremors, wind, etc.) is not expected to affect the resonance frequencies.

Many frequencies of the coupled system are found, which are characterised by both bridge and truck modal displacements. In this work, only the fundamental mode of bridge is of major interest since it is the one commonly used in modal scaling procedure. The canonical mode shape of this mode is reported in Fig. 2**a**. However, in a coupled bridge-trucks dynamic system, as the one investigated here, two modes are characterised by a modal shape which resembles that of the fundamental mode of a bridge, but for one of them the bridge and trucks are moving in phase, while for the other one in counterphase (Fig. 2**a**). Hence, the choice of which of them should be used in the modal scaling procedure is not trivial, especially if OMA is performed by only measuring the output over the bridge deck. Furthermore, the selection of these two modes among all the others is not simple as well and requires the control of all mode shapes.

To support this task, a quantitative parameter is introduced, namely the Participating Relative Mass Ratio (PRMR) of each mode. By partitioning the modal vector $\boldsymbol{\phi}^n$ of the generic n-th mode into sub-vectors $\boldsymbol{\phi}_b^n$ and $\boldsymbol{\phi}_t^n$ collecting components of modal displacements of the beam and trucks, respectively, vectors collecting the PRMR for the vertical and longitudinal directions relative to trucks and bridge are expressed as:

$$\overline{\overline{\mathbf{m}}}_t^n = \sum_{i=1}^{E}\left[\int_0^{L^i}\left(\mathbf{N}^b\boldsymbol{\phi}_b^{n,i^T}\mathbf{M}^i\right)^2 dz + \left(\boldsymbol{\phi}_t^{n,i^T}\overline{\mathbf{M}}^i\right)^2\right]\Big/\sum_{i=1}^{E}\left(\overline{\mathbf{M}}^i\right) \tag{33a}$$

$$\overline{\overline{\mathbf{m}}}_t^{nT} = 2\sum_{i=1}^{E}\left[\int_0^{L^i}\left(\mathbf{N}^b\boldsymbol{\phi}_b^{n,i^T}\mathbf{M}^i\right)^2 dz + \left(\boldsymbol{\phi}_t^{n,i^T}\overline{\mathbf{M}}^i\right)^2\right]\Big/ tr\left[\sum_{i=1}^{E}\left(\overline{\mathbf{M}}^i\right)\right] \tag{33b}$$

$$\overline{\overline{\mathbf{m}}}_b^n = \sum_{i=1}^{E}\left[\int_0^{L^i}\left(\mathbf{N}^b\boldsymbol{\phi}_b^{n,i^T}\mathbf{M}^i\right)^2 dz + \left(\boldsymbol{\phi}_t^{n,i^T}\overline{\mathbf{M}}^i\right)^2\right]\Big/\sum_{i=1}^{E}\left(\mathbf{M}^iL^i\right) \tag{33c}$$

$$\overline{\overline{\mathbf{m}}}_b^{nT} = 2\sum_{i=1}^{E}\left[\int_0^{L^i}\left(\mathbf{N}^b\boldsymbol{\phi}_b^{n,i^T}\mathbf{M}^i\right)^2 dz + \left(\boldsymbol{\phi}_t^{n,i^T}\overline{\mathbf{M}}^i\right)^2\right]\Big/ tr\left[\sum_{i=1}^{E}\left(\mathbf{M}^iL^i\right)\right] \tag{33d}$$

where $\boldsymbol{\phi}_b^{n,i}$ and $\boldsymbol{\phi}_t^{n,i}$ are sub-vectors collecting components of bridge and trucks modal displacements, respectively, relevant to the i-th FE of length L^i, $\mathbf{M}^i$ and $\overline{\mathbf{M}}^i$ are the bridge and truck mass matrices for the i-th element (see Eq. 10 and Eq. 13), and E is the total number of FE. With reference to the vertical displacements, components of vectors $\overline{\overline{\mathbf{m}}}_b^n$ and $\overline{\overline{\mathbf{m}}}_t^n$ express the percentage of the bridge and truck masses mobilized by each vibration mode over the total mass of bridge and trucks (separately). The two searched modes (where bridge and trucks are moving in phase and counterphase) are those characterised by the higher sum of the previously mentioned components (PRMR); this criterion is used for the mode selection.

Exploiting the problem linearity, the system response, in terms of modal parameters, can be presented in a non-dimensional form introducing two non-dimensional parameters: $\overline{m} = m_b/m_t$ and $\overline{\omega} = \omega_b/\omega_t$ that are the ratio between the overall mass of bridge and the overall mass of trucks, and the ratio between the fundamental frequencies of the unloaded bridge and vehicles separately considered, respectively. The non-dimensional presentation of the response quantities allows the generalization of the problem to be studied and permits the analysis of the dynamic coupling phenomenon from a phenomenological point of view.

To this purpose, modal analyses are repeated on the FE model by assuming a constant $\overline{m}$ ratio (for instance, equal to 2.5 in case of pre-stressed RC bridges, which means the bridge mass is 2.5 times the total mass of trucks) and by varying the $\overline{\omega}$ ratio within a plausible range.

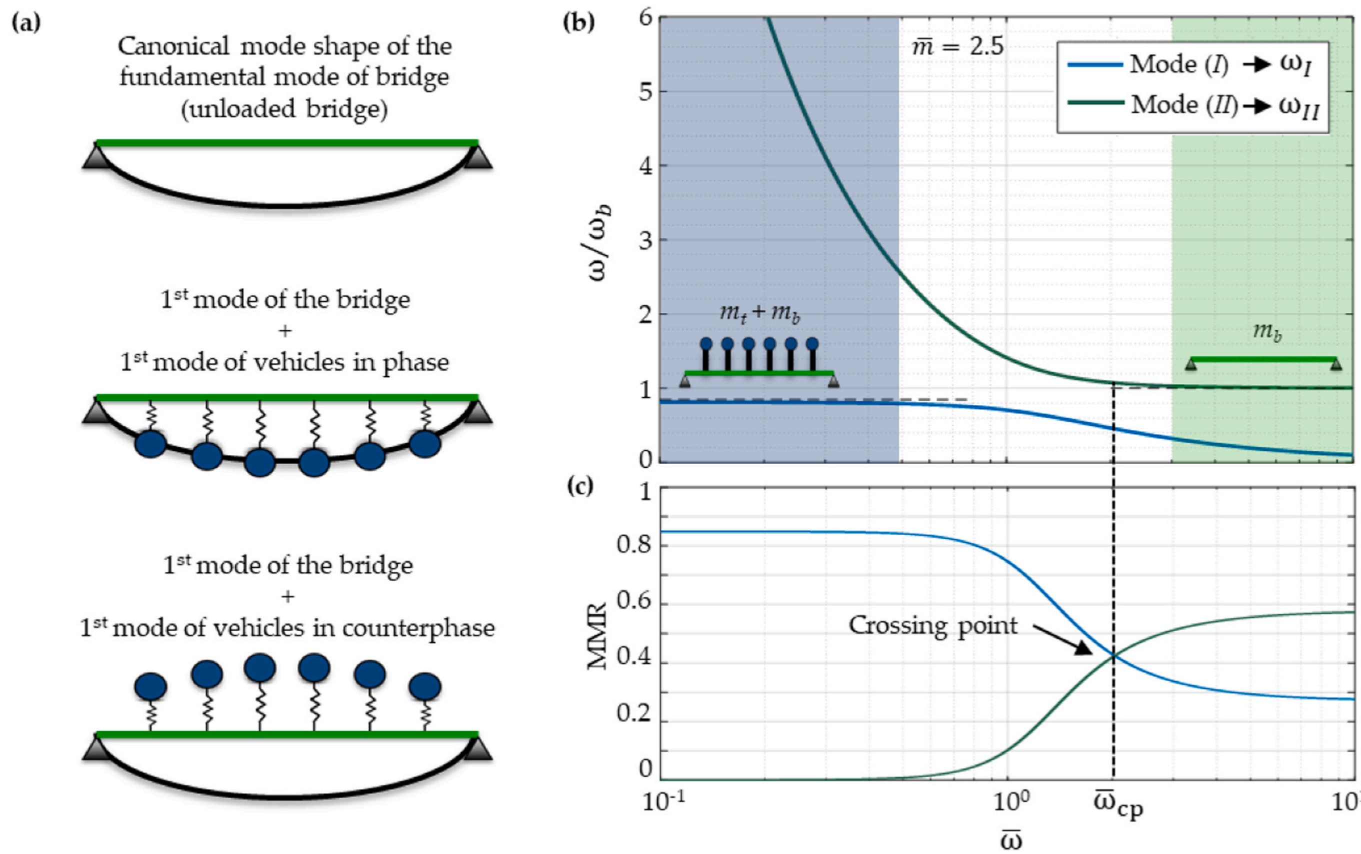

Fig. 2. Phenomenological explanation of the dynamic coupling effect between bridge and vehicles: (a) mode shapes of the considered modes and relevant (b) circular frequency and (c) modal mass ratio (MMR) evolutions.

For each $\overline{\omega}$ ratio, the two modes that maximise the PRMR sum are selected, and the evolution of their circular frequencies is plotted in Fig. 2**b**. The modes are named with mode (*I*), with the lower frequency, and mode (*II*), with the higher frequency. It is worth observing that both frequencies are normalized with respect to the circular frequency of the unloaded bridge (ω_b) in order to facilitate the interpretation of the dynamic coupling effect, as better addressed in the sequel. The dashed black lines represent the circular frequencies of the loaded (left-hand side) and unloaded (right-hand side) bridge when the dynamic coupling effects are neglected, corresponding to values towards the coupled system tends to. Nevertheless, the choice of the mode (*I* or *II*) to be used for the calculation of the frequency shift to be used in the mode scaling process is not trivial. To provide a support in this choice, the MMR ($\overline{\overline{\mathbf{m}}}^n$) for the two selected modes is calculated for the two principal directions, by using the conventional formula:

$$\overline{\overline{\mathbf{m}}}^{nT} = 2\sum_{i=1}^{E}\left[\int_0^{L^i}\left(\mathbf{N}^b\boldsymbol{\phi}_b^{n,i\,T}\mathbf{M}^i\right)^2 dz + \left(\boldsymbol{\phi}_t^{n,i\,T}\overline{\mathbf{M}}^i\right)^2\right] \Bigg/ tr\left[\sum_{i=1}^{E}\left(\mathbf{M}^i L^i + \overline{\mathbf{M}}^i\right)\right] \tag{34}$$

The MMR evolution in the vertical direction for both modes is reported in Fig. 2**c**; the MMR never reaches 100% because of the presence of other vibration modes which are not taken into account. As a general consideration, the mode to be considered in the modal scaling process is the one characterized by the higher MMR for each selected $\overline{\omega}$. From graph in Fig. 2**b**, it is clear that this mode is not always the same: from $\overline{\omega} \cong 0$ to the point where the two MMRs intersect each other (crossing point, approximatively $\overline{\omega}_{cp} = 2$ in this case) mode (*I*) must be used, on the contrary, for higher $\overline{\omega}$ values, mode (*II*).

For a better understanding of the significance of mode (*I*) and (*II*), the acceleration FRFs of the coupled system obtained by applying at the bridge supports a steady state harmonic acceleration of unit amplitude and frequency ω_f, are plotted in Fig. 3. Acceleration FRFs provide a pictorial representation of the dynamic coupling phenomenon because they show the frequency content of the system and they offer qualitatively similar information of the Power Spectral Densities (PSDs) obtained from the analysis of acceleration records from AVTs. FRFs are plotted by retrieving the accelerations at the level of the bridge deck (only the midspan is considered for the sake of simplicity) where sensors are commonly located in performing AVTs. Moreover, a hysteretic damping ratio of 0.25% is also considered with the only intent to avoid asymptotic values for the resonance frequencies, and to make peaks evident.

A comprehensive discussion of Fig. 2**b**, **c** and Fig. 3 allows for an explanation of the importance of the dynamic coupling effects. For $\overline{\omega} < \overline{\omega}_{cp}$, mode (*I*) has higher MMR with respect to mode (*II*), so it must be used in the mass normalization process. Furthermore, this mode is easily identifiable during OMA because it is characterised by a higher amplitude with respect to mode (*II*). Opposite considerations stem from the case $\overline{\omega} > \overline{\omega}_{cp}$, where mode (*II*) must be considered. The task of the mode selection to be used in the mass-change method becomes hard to address when $\overline{\omega} \cong \overline{\omega}_{cp}$, which is the frequency intervals where the dynamic coupling effects have great impact on results interpretation. In Fig. 3, FRFs are complemented by graphs that summarize vertical components of vectors $\overline{\overline{\mathbf{m}}}_b^n$ and $\overline{\overline{\mathbf{m}}}_t^n$ for the two modes. As previously stated, their sum allows the mode selection to be easily performed.

Results presented in Fig. 2**b**, **c**, and Fig. 3 provide a comprehensive and direct indication about the importance of considering the dynamic coupling effects in the dynamic identification of the coupled system. Indeed:

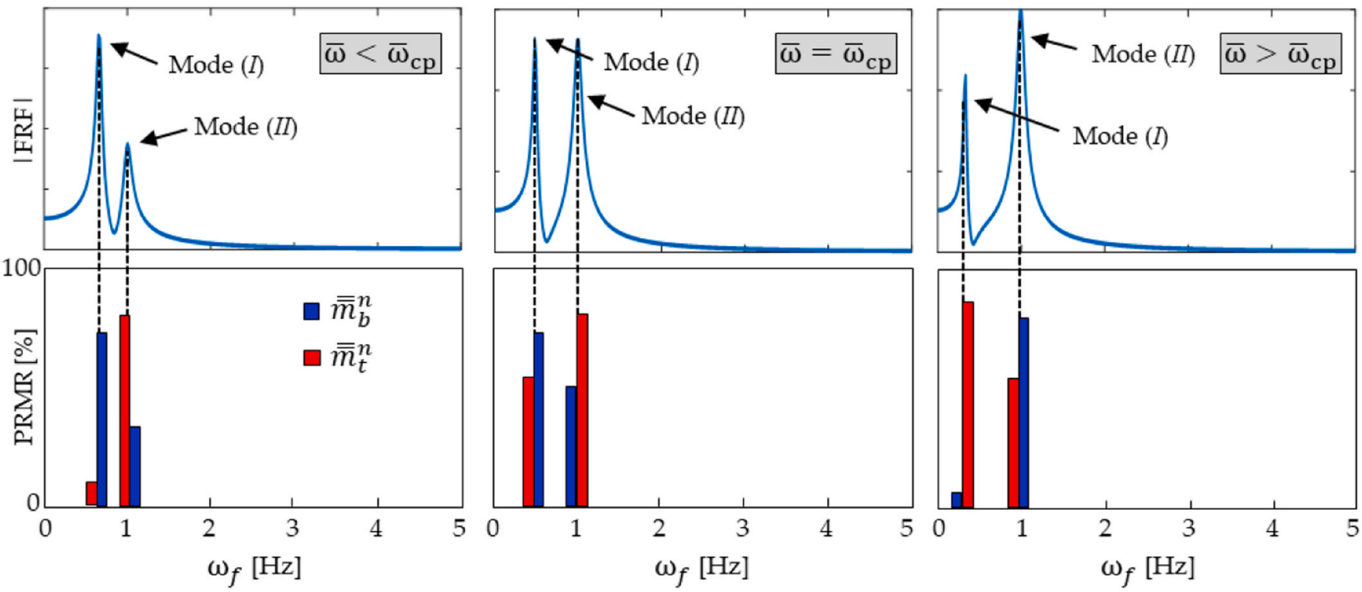

Fig. 3. Acceleration FRFs of the coupled system for three $\overline{\omega}$ ratio casuistries and mode (*I*) and (*II*) selection by using the PRMR sum.

- When $\overline{\omega}$ approaches zero (left-hand side of graphs in Fig. 2**b, c**) the vertical stiffness of trucks is much higher than the flexural stiffness of the bridge; consequently, the coupled system can be reduced to a simple supported beam with truck masses rigidly lying on the deck. This system is characterized by a fundamental circular frequency (mode (*I*)) lower than that of the unloaded bridge ($\omega_I/\omega_b < 1$). In this case, the second circular frequency of the system (i.e., the one relevant to mode (*II*)) tends to infinite and the first mode mobilize the majority of the modal mass (MMR close to 1 in Fig. 2**b**). Consequently, mode (*I*) must be considered for the calculation of the frequency shift. Furthermore, the first peak shown in the FRF of the coupled system (graph on the left in Fig. 3) is associated to mode (*I*) that mainly involves the deflection of the bridge deck ($\overline{\overline{\mathbf{m}}}_b^n >> \overline{\overline{\mathbf{m}}}_t^n$). It is worth noting that in this case, interpretation of data from OMA on real structures is not difficult since one main peak is evident in the spectrum. Above considerations hold for the $\overline{\omega}$ range highlighted with a blue shadow in Fig. 2**b**.
- When $\overline{\omega}$ tends to infinite (right-hand side of graphs in Fig. 2**b, c**) the vertical stiffness of trucks is much lower with respect to the flexural stiffness of the bridge. In this case, the first resonance frequency (mode (*I*)) is very low and is mainly characterised by truck vibrations ($\overline{\overline{\mathbf{m}}}_b^n << \overline{\overline{\mathbf{m}}}_t^n$), while the second resonance frequency (mode (*II*)) is that of the simply supported beam representative of the unloaded bridge, with the fundamental circular frequency almost equal to that of the unloaded bridge ($\omega_{II}/\omega_b \cong 1$). In this case, the second circular frequency (i.e., the one relevant to mode (*II*)) mobilizes the majority of the mass (with a higher MMR in Fig. 2**b**). So, mode (*II*) must be used for the frequency shift determination. The FRF of the system (graph on the right in Fig. 3) shows two peaks with different amplitudes. Generally, the first peak is lower than the second one, which largely involves the deck in terms of modal displacements. In this case, the dynamic coupling effect has negligible influence, and the fundamental frequency of the loaded bridge resembles that of the unloaded bridge. Above considerations hold for the $\overline{\omega}$ range highlighted with a green shadow in Fig. 2**b**.
- When $\overline{\omega}$ is close to the crossing point $\overline{\omega}_{cp}$, the classical response of a tuned system is obtained, and the dynamics of the coupled system is described by two circular frequencies, one lower than that of the loaded bridge (mode (*I*)) and the other one higher than that of the unloaded bridge (mode (*II*)). The FRF of the system (graph in the centre of Fig. 3) shows two peaks that represent the response of a classical tuned mass system. In this case, the selection of the mode to be used in the mass-change method is not an easy task, and the dynamic coupling effect has a non-negligible influence on the interpretation of the system dynamics. However, the mode to be used is the one mobilizing the majority of the MMR, namely, mode (*I*) on the left of the crossing point, and mode (*II*) on the right.

Summarizing, by entering the graphs of Fig. 2**b, c** with a fixed $\overline{\omega}$ ratio (depending on the case at hand), it is possible to have an idea about frequency values that should be expected form OMA performed on the loaded structure. These two frequencies are those relevant to modes with the canonical fundamental mode shape of the bridge deck. So, by using graphs of Fig. 2**b, c** it is possible to evaluate the relevance of the dynamic coupling effects, and to understand which mode should be used in the modal scaling process. To calculate the $\overline{\omega}$ ratio, the fundamental vertical frequency of the unloaded bridge and the vertical one of trucks must be known. The former can be determined through OMA performed on the unloaded structure, while the latter can be found in the scientific literature, or measured on a typical truck (OMA based on AVT recordings).

4. A simple model for the phenomenological analysis of the dynamic coupling effect between bridge and stationed vehicles

A simple model for the investigation of the dynamic coupling effects between bridge and stationed trucks is herein introduced. This model permits to easily and quickly address the dynamic coupling issues between the bridge and stationed trucks. In addition, due to its simplicity, it allows the phenomenological study of the problem to be done, according to a parametric scheme in order to get the problem generalization.

The bridge and vehicles are schematized with a simple 2 Degree of Freedom (2-DoF) system, where m_b and m_t are the overall bridge and truck masses, respectively, and k_t and k_b are the vertical stiffness of trucks and the flexural stiffness of the bridge, respectively (Fig. 4**b**). Each truck is modelled by using a single DoF system (mass and vertical spring) as it is assumed that the roto-translational dynamics of the single multi-axis truck does not significantly influence that of the fundamental mode of the bridge, especially because the spatial footprint of a truck above the deck can often be schematized with good approximation as punctual. So, k_t is the stiffness associated to the first vibration mode of the truck (that is mainly vertical). The resonance frequencies of the

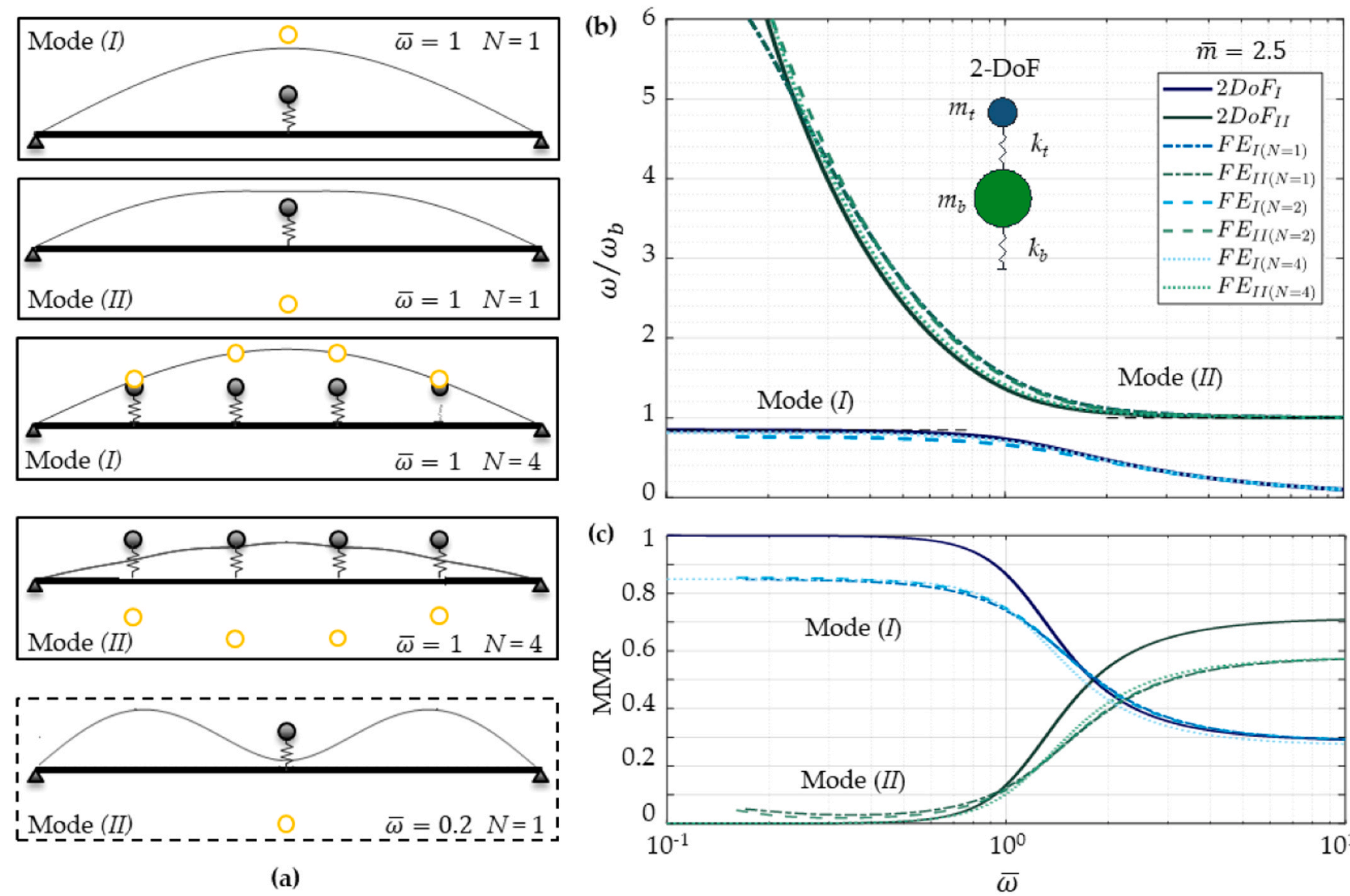

Fig. 4. Results of the 2-DoF system and comparison with FE modelling: (a) mode shapes of the investigated cases (obtained from the FE model), (b) circular frequencies and (c) MMRs of the coupled system obtained from both the 2-DoF and FE models.

coupled 2-DoF system are obtained by considering the following eigenvalue problem:

$$\left(\widetilde{\mathbf{K}} - \omega^2\widetilde{\mathbf{M}}\right)\widetilde{\boldsymbol{\phi}} = \boldsymbol{0} \tag{35}$$

where

$$\widetilde{\boldsymbol{\phi}} = \begin{bmatrix}\phi_t & \phi_b\end{bmatrix}^T \tag{36}$$

is the vector of modal displacements, ω is the natural circular frequency of the system, and

$$\widetilde{\mathbf{K}} = \begin{bmatrix} k_t & -k_t \\ -k_t & k_t + k_b \end{bmatrix}; \quad \widetilde{\mathbf{M}} = \begin{bmatrix} m_t & 0 \\ 0 & m_b \end{bmatrix} \tag{37a,b}$$

are the stiffness and mass matrix of the 2-DoF system, respectively. Eq. 35 has non-trivial solutions if $\det\left[\widetilde{\mathbf{K}} - \omega^2\widetilde{\mathbf{M}}\right] = 0$, and the resulting roots (ω^2) are the circular frequencies of the coupled system. By separately considering the two systems at hand (bridge and vehicles), their fundamental circular frequencies can be written as follows:

$$\omega_t = \sqrt{k_t/m_t}; \quad \omega_b = \sqrt{k_b/m_b} \tag{38a,b}$$

It is worth repeating that ω_b represents the circular frequency of the unloaded bridge. Introducing Eq. 38 in Eq. 35 and after some algebraic manipulations, the 2-DoF system equation of motion becomes:

$$\left\{\begin{bmatrix} 1 & -1 \\ -1 & 1 + \dfrac{m_b\omega_b^2}{m_t\omega_t^2} \end{bmatrix} - \frac{\omega^2}{\omega_t^2}\begin{bmatrix} 1 & 0 \\ 0 & \dfrac{m_b}{m_t} \end{bmatrix}\right\}\begin{bmatrix} 1 \\ \dfrac{\phi_b}{\phi_t} \end{bmatrix} = \mathbf{0} \tag{39}$$

that allows the problem to be formulated in non-dimensional form. By introducing the two parameters $\bar{m}$ and $\bar{\omega}$ defined in Eq. 3, Eq. 39 yields:

$$\left\{\begin{bmatrix} 1 & -1 \\ -1 & 1 + \bar{m}\bar{\omega}^2 \end{bmatrix} - \frac{\omega^2}{\omega_t^2}\begin{bmatrix} 1 & 0 \\ 0 & \bar{m} \end{bmatrix}\right\}\begin{bmatrix} 1 \\ \dfrac{\phi_b}{\phi_b} \end{bmatrix} = \mathbf{0} \tag{40}$$

Eq. 40 has non-trivial solutions if:

$$\det\left\{\begin{bmatrix} 1 & -1 \\ -1 & 1 + \bar{m}\bar{\omega}^2 \end{bmatrix} - \frac{\omega^2}{\omega_t^2}\begin{bmatrix} 1 & 0 \\ 0 & \bar{m} \end{bmatrix}\right\} = 0 \tag{41}$$

Solving Eq. 41, the non-negative non-dimensional circular frequencies of the 2-DoF system (ω_I and ω_{II}) can be calculated as:

$$\left(\frac{\omega}{\omega_b}\right)_{I,II} = \frac{1}{\bar{\omega}}\sqrt{\frac{1 + \bar{m}(1+\bar{\omega}^2) \pm \sqrt{\left(1 + \bar{m}(1+\bar{\omega}^2)\right)^2 - 4\bar{m}^2\bar{\omega}^2}}{2\bar{m}}} \tag{42}$$

Again, the circular frequencies of the 2-DoF system are normalized with respect to the circular frequency of the unloaded bridge (ω_b). Keeping constant $\bar{m}$, the two circular frequencies of the simple 2-DoF system (and the relevant MMRs) can be traced by varying the $\bar{\omega}$ ratio, and graphs similar to those of Fig. 2**b** and **c** can be obtained.

In order to assess the reliability of the simple 2-DoF system in predicting the relevance of dynamic coupling effects between bridge and stationed trucks, results obtained from Eq. 42 are compared with those obtained from the FE model discussed in Section 3. In detail, three typical load layouts, used in common bridge proof load tests, are analysed with the FE model (please, refer to Fig. 5 for the meaning of N): one transverse line of trucks ($N = 1$) in the mid-span of the deck, two ($N = 2$) and four ($N = 4$) transverse lines of trucks centred with respect to the mid-span (Fig. 4**a**); in all cases, to make the comparison feasible, the mass ratio $\overline{m}$ is always assumed equal to 2.5, which is used also for the 2-DoF. Modal analyses are performed by varying the $\overline{\omega}$ ratio between bridge and trucks, and the obtained results are depicted in Fig. 4**b** and **c** in terms of frequencies and MMRs. In this figure, results relevant to the 2-DoF system are reported with continuous lines to facilitate the comparison. As can be observed, frequencies identified by the 2-DoF system are very close to those identified through the refined FE model, and the agreement between the two models is improving passing from $N = 1$ to $N = 4$, i.e., passing from a localized vehicle centred on the bridge deck to a distributed load. However, also the case $N = 1$ provides very satisfactory results. The MMRs denote greater differences with respect to frequencies evolution because of the different distribution of masses; however, differences are not substantial since this parameter is only considered for a qualitative understanding of modes.

Fig. 4**a** also depicts the mode shapes of the FE model when $\overline{\omega} = 1$, for the cases $N = 1$ and $N = 4$. As expected, for $\overline{\omega} = 1$ the mode (*I*) mobilizes the majority of the mass and the relevant mode shape foresees high modal displacements for both bridge and trucks, which move in phase. Mode (*II*) mainly involves the trucks' dynamics (low MMR) and the bridge and trucks move in counterphase. However, it must be said that for very low $\overline{\omega}$ ratios and for mass concentrated in the mid-span (e.g., $N = 1$ and $N = 2$ - bottom picture in Fig. 4**a**) the second mode (i.e., the one mainly involving vehicles) foresees a mode shapes of the bridge quite different from the canonical first mode shape of the bridge, as a consequence of the high stiffness of trucks and the concentrated mass. For this reason, frequencies and MMRs in Fig. 4**b** and **c** relevant to $N = 1$ and $N = 2$ are not reported for very low values of $\overline{\omega}$.

Summarizing, it can be concluded that the accuracy of the 2-DoF system in reproducing the dynamic behaviour of the coupled system is very high since results of this simple model are very similar to those achieved through a refined FE modelling, excluding the cases of concentrated trucks at mid-span and very low values of $\overline{\omega}$. Consequently, the simple 2-DoF system is adopted to develop a parametric analysis with the main target of investigating the dynamic coupling effects arising for load configurations commonly used in proof load tests. The latter are commonly realized by positioning trucks in a non-symmetrical manner with respect to the cross-section of the deck in order to maximize the effects on one of the lateral beams. The simple 2-DoF model does not take this eccentricity into consideration, which however can be considered negligible, especially in the case of common decks with a reduced number of traffic lanes. In case torsional effects become relevant, dedicated load configurations should be considered avoiding eccentricity.

5. Parametric analysis to understand the importance of dynamic coupling effects in real applications

In this Section, a comprehensive parametric investigation is carried out to numerically investigate the influence of dynamic coupling effects between bridge and stationed trucks on the dynamic identification of bridges loaded with different stationed truck layouts. The parametric analysis is performed adopting the 2-DoF system and focusing on two common bridge construction typologies widely adopted worldwide, namely concrete (pre-stressed) and steel-concrete composite bridges. As previously stated, parameters governing the bridge-trucks system dynamics are $\overline{m}$ and $\overline{\omega}$ ratios. The analytical model has been formulated assuming $\overline{\omega}$ as the independent variable and fixing $\overline{m}$, the latter considered as a known parameter; so, the influence of $\overline{m}$ needs to be investigated. The basic idea is that of studying effects of dynamic coupling effects between bridge and trucks arising for different load layouts typically adopted in bridge proof load tests in order to be able to exploit proof load tests as an occasion to perform OMA on the unloaded and loaded bridge in order to apply the mass-change method for estimating the modal scale factors.

5.1. Determination of common $\overline{m}$ ratios in bridge proof load tests

The $\overline{m}$ ratio mainly depends on three parameters, which are the number of longitudinal (l) and transverse (N) lines of trucks positioned over the deck, and the $\overline{L}$ ratio ($\overline{L} = L_{ld}/L$), defined as the ratio between the length of the loaded deck (L_{ld}) and the total length of the bridge span (L). In the parametric analysis, these parameters are assumed on the basis of the most common cases that can be encountered in the practice for bridge proof load testing. For what concerns the first two parameters, l from 1 to 3 is considered, as well as N equal to 1, 2 and 4, as shown in Fig. 5. Then, three $\overline{L}$ ratios are taken into consideration, equal to 0.25, 0.50 and 0.75, meaning that 25%, 50% and 75% of the span length is loaded with trucks. Assuming a common truck length of 10 m and considering the three cases of N reported in Figs. 5, 9 different span lengths can be calculated reversing the $\overline{L}$ ratio formula (Fig. 6); however, one of the latter, with length of 160 m, is excluded from the applications since it is not representative of common composite and concrete bridges. Hence, combining cases of Fig. 5 with those of Fig. 6, 24 typical loaded bridge layouts are obtained, reported in Table 1. It is worth pointing out that for pre-stressed RC decks, span length of 80 m is impractical, and it is herein considered only in order to explore the dynamic coupling phenomenon for an upper bound limit.

For each construction typology, other two sub-classes are considered on the basis of the structural typology, namely I-beam girder and box-girder decks. Starting from steel-concrete composite structures, a rough estimation of the steel carpentry weight is obtained based on the

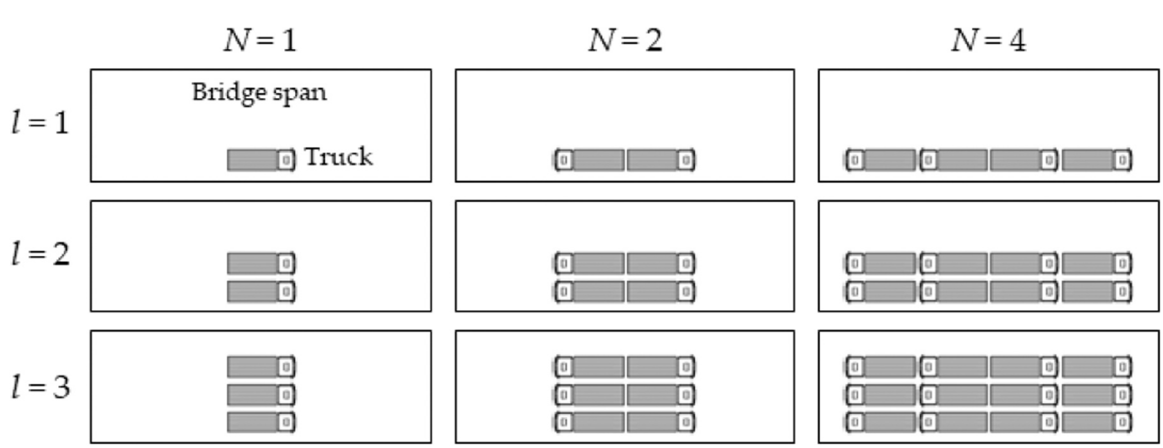

Fig. 5. Common truck layouts over a bridge deck for proof load tests.

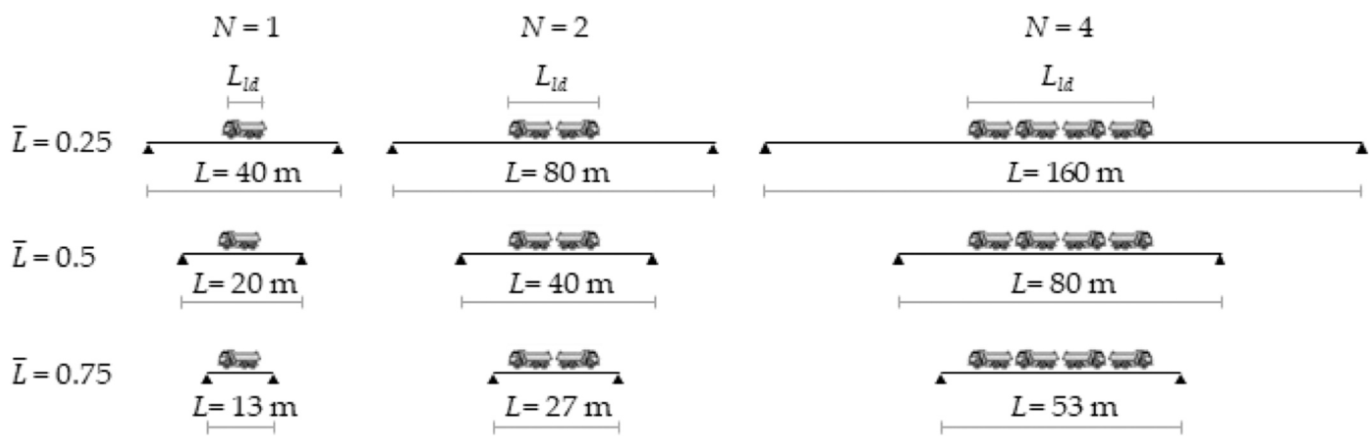

Fig. 6. Considered span length based on the number of trucks on a single line (*N*).

Table 1
Typical bridge loading layouts considered for the parametric analysis.

Layout	$\bar{L}$	*N*	*l*	*L* [m]
1	0.25	1	1	40
2	0.25	1	2	40
3	0.25	1	3	40
4	0.25	2	1	80
5	0.25	2	2	80
6	0.25	2	3	80
7	0.5	1	1	20
8	0.5	1	2	20
9	0.5	1	3	20
10	0.5	2	1	40
11	0.5	2	2	40
12	0.5	4	2	80
13	0.5	4	3	80
14	0.75	1	1	13
15	0.5	2	3	40
16	0.5	4	1	80
17	0.75	1	2	13
18	0.75	1	3	13
19	0.75	2	1	27
20	0.75	2	2	27
21	0.75	2	3	27
22	0.75	4	1	53
23	0.75	4	2	53
24	0.75	4	3	53

span length and by adopting the following formulations [37]:

$$q\left[kg/m^2\right] = 0.105L^{1.6} + 100 \quad \text{For twin} - \text{girder decks} \tag{43a}$$

$$q\left[kg/m^2\right] = 2.85L + 45 \quad \text{For box} - \text{girder decks} \tag{43b}$$

The weight of the concrete slab, calculated assuming a slab thickness of 25 cm and width of 12 m, is added to loads obtained through Eq. 43. For what concerns the pre-stressed RC decks, their weight is roughly estimated starting from I-beam and box-girder cross-sections of real case studies (decks width of about 12 m) and increasing their height as the span length increases, keeping constant the ratio between the span length and the cross-section height. The total bridge weight for all construction typologies is finally achieved adding the non-structural loads (road pavement, barriers, and kerbs). The obtained values are reported in Table 2 as a function of the construction typology and bridge span length. By combining the 24 bridge loading layouts (Table 1) with the four chosen construction typologies, 96 $\overline{m}$ values are obtained and, assuming the truck mass equal to 40 t (a typical value for common trucks used in proof load tests), the $\overline{m}$ ratio varies between 1.00 and 9.36. It is noteworthy that the use of the non-dimensional parameter $\overline{m}$ has the great advantage to allow for the analysis of the coupled system regardless the bridge span length, which is indirectly considered within

Table 2
Linear weight [kN/m] for the considered bridge decks.

L [m]	Steel-concrete composite		Pre-stressed RC	
	Twin-girder	Box-girder	I-beam girder	Box-girder
13.3	118.3	115.4	122.3	120.1
20	119.0	117.7	143.3	153.0
27	120.0	120.0	172.7	164.9
40	122.1	124.6	256.7	183.3
53	124.8	129.1	374.2	195.6
80	131.4	138.2	—	275.6

that parameter.

5.2. Effects of $\overline{m}$ ratio variation on the dynamic coupling effect between bridge and trucks

Starting from the range of $\overline{m}$ defined in the previous section, the following set of values has been chosen to perform the parametric analysis, spanning the interval between minimum and maximum possible values: $\overline{m}$ = 1, 2, 3, 4, 5 and 10. These selected values are adopted in the calculation of the frequencies of the coupled systems (ω_I and ω_{II} using Eq. 42), and results are plotted in Fig. 7. As previously stated, the dynamic coupling effect has influence on the interpretation of the system dynamics when $\overline{\omega}$ ratio is around the crossing point of MMR ($\overline{\omega}_{cp}$). Observing Fig. 7**b** it is evident that the $\overline{\omega}_{cp}$ increases by decreasing the $\overline{m}$ ratio, i.e., when the mass of vehicles becomes comparable to that of the bridge. Observing Fig. 7**a** it is also possible to note that the distance between the several $\overline{m}$ ratio curves rapidly reduces if $\overline{m}$ increases, and becomes almost negligible for $\overline{m}$ ratios greater than 3 (i.e., truck masses lower than 33% of the bridge span mass). Since graphs of Fig. 7 have been determined considering a realistic set of $\overline{m}$ ratios, they can be adopted to investigate the dynamic coupling effects in the dynamic identification of real steel-concrete composite and pre-stressed RC bridges. By entering the graphs with the actual $\overline{\omega}$ value and considering the $\overline{m}$ curve for the loaded bridge at hand, it is possible to verify whether or not the dynamic coupling effect has a significant influence in the dynamic identification; besides, frequencies and MMRs expected during the proof load test can be estimated as well. Interpolation is possible for $\overline{m}$ ratios not reported in graphs.

In the framework of the mass-change method, graphs of Fig. 7 are a graphical tool for experimentally estimating the bridge frequency to be used in the mass-change method applied to the fundamental vibration mode of simply supported decks. A broad description of the procedure to be performed and how to use these graphs is reported in Section 6.

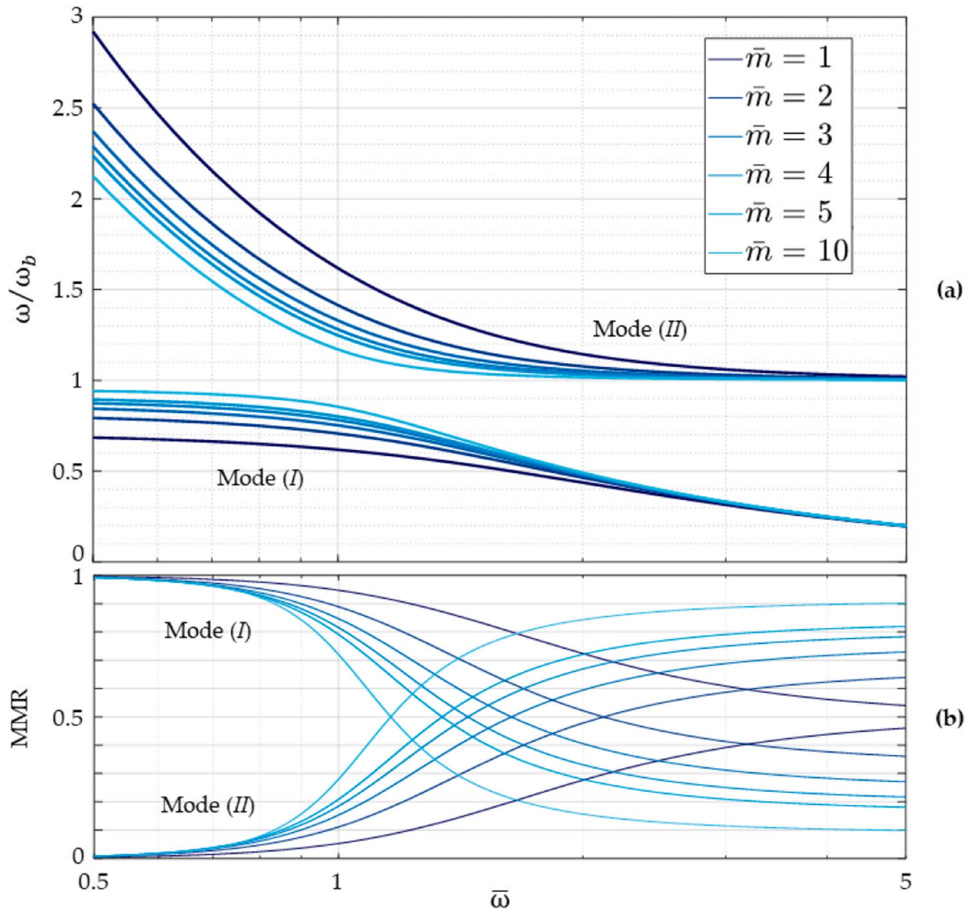

Fig. 7. Generalized graphs for the interpretation of bridge-trucks dynamic coupling effects: (a) circular frequency evolutions of mode (*I*) and (*II*) and (b) MMRs as a function of $\overline{m}$ ratio.

5.3. Steady state response of the 2-DoF system

As already stated, the acceleration FRFs can be conveniently studied to better understand the dynamic coupling phenomena. In this Section, the acceleration FRFs obtained by applying a steady state harmonic acceleration of unit amplitude at the base of the 2-DoF analytical model, and by retrieving accelerations at the level of the bridge deck, are shown. As done in Section 3, a low hysteretic damping ratio of 0.25% is considered to avoid numerical asymptotic values for the resonance frequencies and to make peaks clearly evident. FRFs are calculated by varying the forcing circular frequency ω_f of the harmonic acceleration within the range 0 - 2.5ω_b, and assuming (for instance) $\overline{m} = 2$.

The obtained FRFs are drawn in Fig. 8 with continuous blue lines of different shades. They are divided into three graphs: the left-hand side graph reports all the FRFs obtained assuming $\overline{\omega}$ ratio values lower than that corresponding to the crossing point ($\overline{\omega}_{cp}$), the right-hand side graph collects the FRFs considering $\overline{\omega}$ ratios greater than $\overline{\omega}_{cp}$, and the middle graph is obtained assuming $\overline{\omega} = \overline{\omega}_{cp}$. The light blue continuous lines in the left-hand side refers to $\overline{\omega} \ll \overline{\omega}_{cp}$, while in the right-hand side refer to $\overline{\omega} \gg \overline{\omega}_{cp}$. FRFs depicted with a dashed red line refer to the unloaded bridge (1-DoF), while those relevant to the bridge where trucks are only considered in terms of added mass are reported for comparison with a

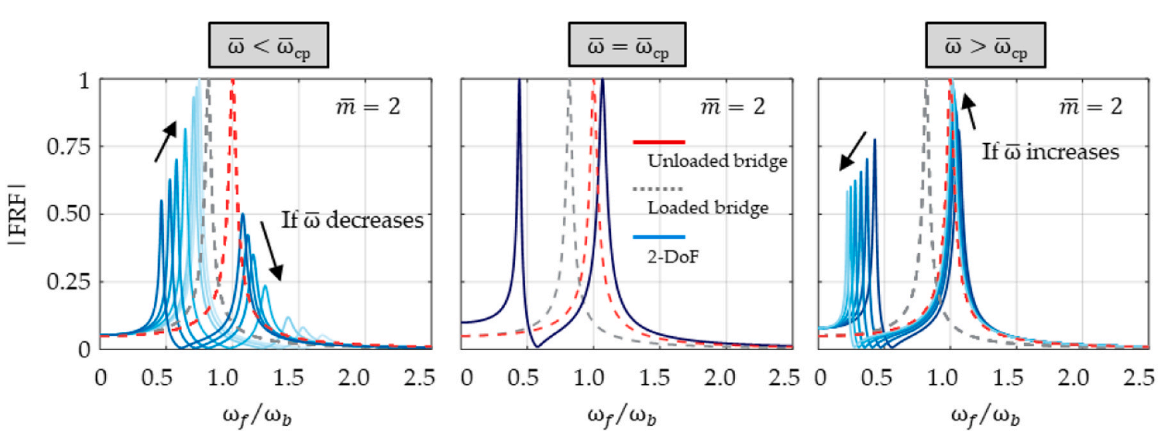

Fig. 8. Acceleration FRFs of the coupled 2-DoF system determined considering three representative $\overline{\omega}$ ratio intervals.

dashed grey line. For $\overline{\omega} < \overline{\omega}_{cp}$ (left-hand side graph), FRFs of the 2-DoF system show the first peak (mode (*I*)) in correspondence of frequency values lower than that of the unloaded bridge (ω_b). When $\overline{\omega}$ is similar to $\overline{\omega}_{cp}$ peaks relevant to mode (*I*) and (*II*) have similar amplitudes, then, when $\overline{\omega}$ reduces, the peak relevant to mode (*I*) rapidly increases while that relevant to mode (*II*) decreases and moves to higher frequencies, demonstrating that, in these cases, the dynamic coupling effect can be neglected since result interpretation from OMA becomes easy and unambiguously. For $\overline{\omega} > \overline{\omega}_{cp}$ (right-hand side graph), FRFs of the 2-DoF system show peaks of mode (*II*) with amplitude and frequencies comparable to that of the unloaded bridge, while peaks of mode (*I*) firstly have similar amplitude, then, when $\overline{\omega}$ ratio increases, they decrease in amplitude and move towards lower frequencies. However, differently from the case $\overline{\omega} < \overline{\omega}_{cp}$, peaks of mode (*I*) do not become very low in amplitude, meaning that the dynamic identification from OMA needs to be carefully done and taking into account the dynamic coupling effects between the two systems.

Summarizing, in some cases the application of the mass-change method using modal parameters obtained from OMA performed during proof load tests requires some preliminary operations in order to compensate effects of the dynamic coupling between bridge and trucks.

6. Application of the mass-change method from OMA performed during proof load tests

6.1. Suggested procedure for the determination of the frequency shift

In this Section, a methodology to account for the dynamic coupling effects among bridge and stationed trucks in mass-change method application and exploiting OMA performed during proof load tests, is presented. Steps of the proposed methodology, schematized in Fig. 9, are commented below, with some practical suggestions.

1) The bridge is dynamically tested in its unloaded condition (referred to be the "0" condition) and placing sensors (e.g., accelerometers or velocimeters) in the established points (e.g., red dots in Fig. 9), in order to capture the structure dynamics with the desired accuracy. After OMA, the fundamental frequency of the unloaded structure is determined (ω_b corresponding to ω_0 in Section 2), together with its modal shape vector ($\boldsymbol{\phi}_0$). It is required that at least some sensors are placed in the same positions in which trucks will be located in subsequent tests. The total mass of the bridge (m_b, required for the calculation of the $\overline{m}$ ratio) can be easily estimated from the design drawings or the numerical model.
2) The bridge is loaded with trucks, e.g., during load testing procedures. Typically, trucks used in this occasion are very similar to each other and, consequently, they are assumed to be identical. The mass of trucks (m_t) is known, being the vehicles weighed before their use, while their frequency can be experimentally measured or assumed from the technical literature (in fact, it is reasonable to expect that similar types of trucks also have similar mechanical characteristics, having to satisfy particular design standards). The characteristics of trucks, together with those of the bridge, are used for the calculation of $\overline{m}$ and $\overline{\omega}$ ratios. The role of the load layout will be addressed in the sequel. OMA is performed on the loaded bridge (referred to be the "1" condition). As deeply discussed in the manuscript, in this case the experimental identification of the fundamental mode could be non-trivial, especially in cases where dynamic coupling effects among the two systems are non-negligible. The worst situation is achieved for $\overline{\omega} = \overline{\omega}_{cp}$, for which the bridge loaded with trucks has two frequencies to which the canonical first vibration mode shape is associated ($\omega_{1,I}$ and $\omega_{1,II}$).
3) The mode to be considered for the calculation of the frequency shift for modal scaling is determined by using graphs of Fig. 7. By entering the graphs with the calculated $\overline{\omega}$ ratio for the case study at hand and intersecting the curves relevant to the considered mass ratio $\overline{m}$, the two frequencies characterized by the canonical first vibration mode shape of the bridge are found ($\omega_{1,I}/\omega_b$ and $\omega_{1,II}/\omega_b$, relevant to mode (*I*) and (*II*), respectively). To determine the one to be used in the calculation of the frequency shift, the graph of the MMR is adopted: the mode with the greater MMR must be considered.
4) The frequency value obtained intersecting the curve of Fig. 7 cannot be directly used for the calculation of the frequency shift because it is affected by the dynamic coupling effect between bridge and trucks. Indeed, for the mass-change method, the frequency to be used is the one referring to the loaded bridge with only masses (rigid loads). At first, the term $\Delta\omega_1$, defined as:

$$\Delta\omega_1 = \frac{\omega_1}{\omega_b} - \frac{\omega_{1,I}}{\omega_b} \tag{44}$$

has to be determined from the graph, from which

$$\frac{\omega_1}{\omega_b} = \Delta\omega_1 + \frac{\omega_{1,I}}{\omega_b} \tag{45}$$

can be computed. Finally, the resonance frequency of the bridge ω_1 cleansed from the truck compliance can be evaluated according to:

$$\omega_1 = \omega_b\left(\Delta\omega_1 + \frac{\omega_{1,I}}{\omega_b}\right) \tag{46}$$

in which ω_b is the fundamental frequency of the unloaded bridge determined at the beginning (i.e., $\omega_b = \omega_0$), $\Delta\omega_1$ is determined by using graphs of Fig. 7, and $\omega_{1,I}$ is experimentally identified testing the loaded bridge and with the support of graphs of Fig. 7.
5) The mass-change method can be applied using ω_b for the unloaded bridge and ω_1 for the loaded bridge, obtaining the scaling factor α for the mass normalization of modes.

6.2. Influence of truck masses and load layouts on the correct evaluation of the mass-normalized mode shapes

One of the basic requirements for the use of the mass-change method is that the mode shape of the investigated vibration mode in the loaded configuration does not sensibly vary from the relevant one in the unloaded condition. In order to investigate this issue, several truck masses and locations over the deck are numerically investigated and their suitability in being used in the mass-change method is addressed exploiting the FE model introduced in Section 3. In detail, three truck layouts are considered, corresponding to typical load layouts of real proof load tests ($N = 1$, $N = 2$, $N = 4$), while the mass of trucks is varied changing the $\overline{m}$ ratio from 1 to 10 (Fig. 10**a**). In this case, the $\overline{\omega}$ ratio is not varied because, as previously shown, it may affects the modal identification of the loaded bridge but not the mass-change method outcomes since it only depends on the added masses and the mass layouts. Consequently, thirty cases are considered; for each of them, the frequency of the fundamental vibration mode (ω_1) to be used in the calculation of the scaling factor α is obtained exploiting the procedure addressed in Section 6.1.

To assess the goodness of scaled mode shapes, the respect of the orthogonality condition is used, i.e., $\alpha\boldsymbol{\phi}_0^T\mathbf{M}\alpha\boldsymbol{\phi}_0 = 1$; results are reported in Fig. 10**b**. As can be observed, the orthogonality condition is almost always satisfied, with a little loss of accuracy when the mass becomes gradually concentrated to the mid-span and when the mass of trucks becomes large enough to approach that of the bridge. Above conditions are responsible for a modification of the mode shape of the loaded bridge with respect to that of the unloaded one, although almost negligible.

To further assess changes of the loaded mode shape with respect to the unloaded relevant one, the Modal Assurance Criterion (MAC) [38] index is calculated between the two mode shapes ($\boldsymbol{\phi}_0$ and $\boldsymbol{\phi}_1$). Results are reported in Fig. 10c. Again, it can be asserted that results are always

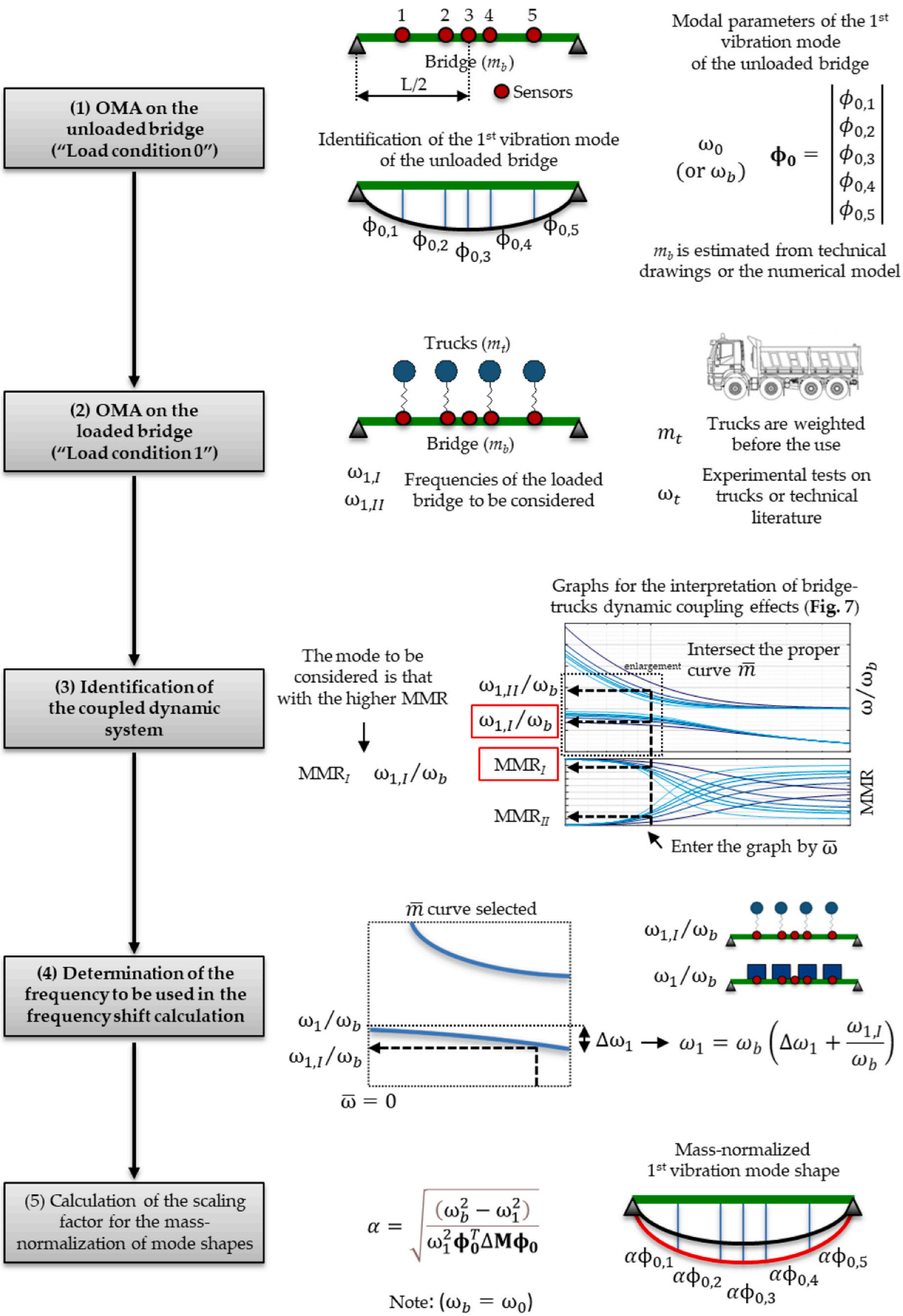

Fig. 9. Flowchart of the procedure for obtaining mass-normalized mode shapes considering the dynamic coupling effects between bridge and stationed trucks.

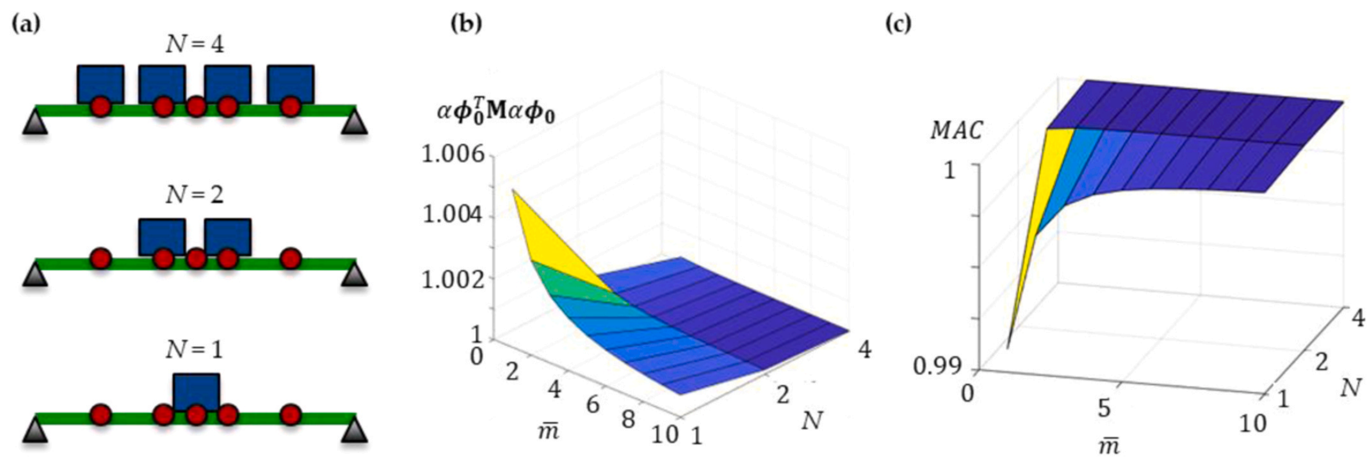

Fig. 10. Influence of mass and layout of trucks in the variation of the loaded mode shape: (a) considered load casuistries, (b) assessment of mass-normalized mode shapes in terms of the orthogonality condition and (c) MAC index.

satisfying, with little variation of mode shapes for the cases discussed above.

7. Conclusions

The paper discussed about the correct determination of frequency shift to be used in the mass-change method for experimentally obtaining mass-normalized mode shapes of bridges loaded with stationed vehicles. Indeed, it has been demonstrated that in some cases the experimental dynamic identification (OMA) of bridges loaded with stationed vehicles is not straightforward because of the dynamic coupling effects arising between the coupled system constituted by the bridge and trucks. Issues relevant to the modal identification of bridges loaded with stationed trucks were firstly addressed by adopting a FE model in which the bridge was modelled as a Euler Bernoulli beam, while trucks were schematised with mass-spring systems. The FE model allowed for a general and non-dimensional discussion of the topic, and situations in which the dynamic coupling effects must be considered or can be neglected were argued. In particular, it has been shown that two vibration modes of interest can be identified, characterised by the canonical fundamental mode shape of the unloaded bridge deck; the choice of the proper mode to be used in the mass-change method can be based on considerations based on the modal mass ratios, namely on the amount of the bridge mass participating to the two modes. In addition, situations characterised by negligible coupling effects are also identified and discussed; in these cases, the dynamic identification is straightforward and there are not concerns in the determination of the fundamental mode of the bridge. As a general conclusion it can be asserted that the influence of the dynamic coupling effects strongly affect the interpretation of the bridge dynamics when the modal mass ratios of the two modes approach the crossing point, namely when the modal mass ratios of these two modes are almost equal, while it can be neglected in other cases.

In order to extend the phenomenological investigation of the problem, a simple but effective 2-DoF system is introduced and analysed in a non-dimensional form, by preliminary validating its reliability comparing results obtained from the refined FE model. The simple model is used to perform a parametric investigation obtaining two graphical tools to be used for the application of the mass-change method starting from OMA performed during proof load tests on bridges. The procedure to obtain the correct frequency shift for the determination of mass-normalized mode shapes was also proposed and illustrated. However, it is worth noting that the proposed tools for supporting the dynamic identification of the coupled system were developed considering a simply supported static scheme of the deck and taking into account only the fundamental mode of the bridge deck. Furthermore, for a clear understanding of the frequency shift, the modes of the deck should be well separated. The proposed procedure can be also applied to other casuistries, although in these cases, the simplified tools can no longer be used, but the loaded structure should be modelled using the proposed FE model, which allows different cases to be considered in addition to the one dealt with in this work.

Finally, some considerations are made concerning the load configurations that can be adopted with the aim of applying the mass-change method and the accuracy of the proposed approach is presented and discussed. It was found that a little loss of precision of the approach is expected when masses are concentrated to the mid-span and, moreover, when the added mass approach that of the bridge. However, this is a very unusual load configuration in practice.

As a general conclusion, it has been demonstrated that mass-normalized mode shapes can be experimentally obtained in bridges exploiting vehicles as added masses on the deck. In case of new bridges, which require a static proof load test, as well as a dynamic test before the opening to traffic, tests for the evaluation of the mass-normalised mode shapes can be almost considered cost-free because of the availability of weighted trucks and the possibility to exploit load configurations used for the static tests. In case of existing bridges, the tests require lower costs with respect to those involving the use of static mass deployed on the deck. Furthermore, it is worth remembering that normalised-mode shapes can be used to define the receptance matrix of the deck, providing a relationship between the measured acceleration and the input accelerations, that are unknown in ambient vibration tests.

Fundings

This research did not receive any specific grant from funding agencies in the public, commercial, or not-profit sectors.

CRediT authorship contribution statement

Vanni Nicoletti: Writing – original draft, Methodology, Investigation, Conceptualization. **Sandro Carbonari:** Writing – review & editing, Validation, Software, Methodology, Conceptualization. **Fabrizio Gara:** Writing – review & editing, Validation, Supervision, Project administration, Conceptualization. **Riccardo Martini:** Visualization, Software, Methodology, Investigation, Formal analysis.

Declaration of Competing Interest

The authors declare that they have no known competing financial interests or personal relationships that could have appeared to influence the work reported in this paper.

Data availability

Data will be made available on request.

Acknowledgements

This work is developed within the research project PROTECT: maPping the seismic Risk Of straTEgiC consTructions (2019–2022). The project received fundings from the Fondazione Cariverona and Fondazione Cassa di Risparmio di Padova e Rovigo, under grant agreement ID 10758 and Cod. SIME 2018.0853.2019.

References

[1] Abarca A, Monteiro R, O'Reilly GJ. Simplified indirect loss characterization for the seismic risk assessment of roadway bridge networks. SSRN Electron J 2021. https://doi.org/10.2139/ssrn.3993198.

[2] Perdomo C, Abarca A, Monteiro R. Estimation of seismic expected annual losses for multi-span continuous RC bridge portfolios using a component-level approach. J Earthq Eng Apr. 2022;vol. 26(6):2985–3011. https://doi.org/10.1080/13632469.2020.1781710.

[3] The Manual for bridge evaluation. 3rd edition.,. Washington, D.C.: American Association of State Highway and Transportation Officials,; 2018.

[4] Cunha Á, Caetano E, Magalhães F, Moutinho C. Dynamic identification and continuous dynamic monitoring of bridges: different applications along bridges life cycle. Struct Infrastruct Eng Apr. 2018;vol. 14(4):445–67. https://doi.org/10.1080/15732479.2017.1406959.

[5] Rainieri C, et al. Shaking table tests for the experimental verification of the effectiveness of an automated modal parameter monitoring system for existing bridges in seismic areas. Struct Control Health Monit 2018;vol. 25(7):e2165. https://doi.org/10.1002/stc.2165.

[6] Brandt A, Berardengo M, Manzoni S, Vanali M, Cigada A. Global scaling of operational modal analysis modes with the OMAH method. Mech Syst Signal Process Feb. 2019;vol. 117:52–64. https://doi.org/10.1016/j.ymssp.2018.07.017.

[7] Philips Adewuyi A, Wu Z, Kammrujaman Serker NHM. Assessment of vibration-based damage identification methods using displacement and distributed strain measurements. Struct Health Monit Nov. 2009;vol. 8(6):443–61. https://doi.org/10.1177/1475921709340964.

[8] Bernagozzi G, Mukhopadhyay S, Betti R, Landi L, Diotallevi PP. Output-only damage detection in buildings using proportional modal flexibility-based deflections in unknown mass scenarios. Eng Struct Jul. 2018;vol. 167:549–66. https://doi.org/10.1016/j.engstruct.2018.04.036.

[9] Yan A, Golinval J-C. Structural damage localization by combining flexibility and stiffness methods. Eng Struct Oct. 2005;vol. 27(12):1752–61. https://doi.org/10.1016/j.engstruct.2005.04.017.

[10] 'A comparison of strain and classic experimental modal analysis - Tadej Kranjc, Janko Slavič, Miha Boltežar, 2016′. Accessed: Nov. 02, 2023. [Online]. Available: https://journals.sagepub.com/doi/10.1177/1077546314533137

[11] Carbonari S, Dezi F, Arezzo D, Gara F. A methodology for the identification of physical parameters of soil-foundation-bridge pier systems from identified state-space models. Eng Struct Mar. 2022;vol. 255:113944. https://doi.org/10.1016/j.engstruct.2022.113944.

[12] Zhang CD, Xu YL. Structural damage identification via multi-type sensors and response reconstruction. Struct Health Monit Nov. 2016;vol. 15(6):715–29. https://doi.org/10.1177/1475921716659787.

[13] Pozzi M, Der Kiureghian A. Response spectrum analysis for floor acceleration. Earthq Eng Struct Dyn 2015;vol. 44(12):2111–27. https://doi.org/10.1002/eqe.2583.

[14] Xue M-S, Yi T-H, Qu C-X, Li H-N. Bridge Flexibility Identification through a Reference-Free Substructuring Integration Method Driven by Mode Fitting. J Eng Mech Mar. 2022;vol. 148(3):04021164. https://doi.org/10.1061/(ASCE)EM.1943-7889.0002082.

[15] R. Brincker, P. Andersen, and N.J. Vej, 'A Way of Getting Scaled Mode Shapes in Output Only Modal Testing'.

[16] Bernal D. Modal Scaling from Known Mass Perturbations. J Eng Mech Sep. 2004; vol. 130(9):1083–8. https://doi.org/10.1061/(ASCE)0733-9399(2004)130:9(1083).

[17] Coppotelli G. On the estimate of the FRFs from operational data. Mech Syst Signal Process Feb. 2009;vol. 23(2):288–99. https://doi.org/10.1016/j.ymssp.2008.05.004.

[18] López-Aenlle M, Fernández P, Brincker R, Fernández-Canteli A. Scaling-factor estimation using an optimized mass-change strategy. Mech Syst Signal Process Jul. 2010;vol. 24(5):1260–73. https://doi.org/10.1016/j.ymssp.2009.06.011.

[19] Bernal D. A receptance based formulation for modal scaling using mass perturbations. Mech Syst Signal Process Feb. 2011;vol. 25(2):621–9. https://doi.org/10.1016/j.ymssp.2010.08.004.

[20] Weijtjens W, De Sitter G, Devriendt C, Guillaume P. Relative scaling of mode shapes using transmissibility functions. Mech Syst Signal Process Oct. 2013;vol. 40(1):269–77. https://doi.org/10.1016/j.ymssp.2013.04.007.

[21] Khodayari R, Bahar O, Ghafory-Ashtiany M. Identification of structural matrices of shear buildings using ambient vibration tests with incomplete measurements. Iran J Sci Technol Trans Civ Eng Dec. 2020;vol. 44(4):1057–74. https://doi.org/10.1007/s40996-019-00323-6.

[22] López-Aenlle M, Brincker R, Pelayo F, Canteli AF. On exact and approximated formulations for scaling-mode shapes in operational modal analysis by mass and stiffness change. J Sound Vib Jan. 2012;vol. 331(3):622–37. https://doi.org/10.1016/j.jsv.2011.09.017.

[23] Khatibi MM, Ashory MR, Malekjafarian A, Brincker R. Mass–stiffness change method for scaling of operational mode shapes. Mech Syst Signal Process Jan. 2012;vol. 26:34–59. https://doi.org/10.1016/j.ymssp.2011.07.012.

[24] Parloo E, Verboven> P, Guillaume P, Van Overmeire M. 'SENSITIVITY-BASED OPERATIONAL MODE SHAPE NORMALISATION'. Mech Syst Signal Process Sep. 2002;vol. 16(5):757–67. https://doi.org/10.1006/mssp.2002.1498.

[25] Parloo E, Cauberghe B, Benedettini F, Alaggio R, Guillaume P. Sensitivity-based operational mode shape normalisation: Application to a bridge. Mech Syst Signal Process Jan. 2005;vol. 19(1):43–55. https://doi.org/10.1016/j.ymssp.2004.03.009.

[26] He W-Y, Ren W-X, Zuo X-H. Mass-normalized mode shape identification method for bridge structures using parking vehicle-induced frequency change. Struct Control Health Monit 2018;vol. 25(6):e2174. https://doi.org/10.1002/stc.2174.

[27] Tian Y, Zhang J, Han Y. Structural scaling factor identification from output-only data by a moving mass technique. Mech Syst Signal Process Jan. 2019;vol. 115:45–59. https://doi.org/10.1016/j.ymssp.2018.05.040.

[28] M. Sheibani, A.H. Hadjian-Shahri, and A.K. Ghorbani-Tanha, 'Mass Scaling of Mode Shapes Based on the Effect of Traffic on Bridges: A Numerical Study', in *Dynamics of Civil Structures, Volume 2*, J. Caicedo and S. Pakzad, Eds., in Conference Proceedings of the Society for Experimental Mechanics Series. Cham: Springer International Publishing, 2017, pp. 95–106. doi: 10.1007/978-3-319-54777-0_13.

[29] Sheibani M, Ghorbani-Tanha AK. Obtaining mass normalized mode shapes of motorway bridges based on the effect of traffic movement. Structures Oct. 2021; vol. 33:2253–63. https://doi.org/10.1016/j.istruc.2021.05.056.

[30] Cantero D, Hester D, Brownjohn J. Evolution of bridge frequencies and modes of vibration during truck passage. Eng Struct Dec. 2017;vol. 152:452–64. https://doi.org/10.1016/j.engstruct.2017.09.039.

[31] Heng K, Li R, Li Z, Wu H. Dynamic responses of highway bridge subjected to heavy truck impact. Eng Struct Apr. 2021;vol. 232:111828. https://doi.org/10.1016/j.engstruct.2020.111828.

[32] Wang H, Nagayama T. Response spectrum model of vehicle dynamic load for the prediction of bridge vibration level due to single vehicle-passage. Eng Struct Jun. 2022;vol. 260:114180. https://doi.org/10.1016/j.engstruct.2022.114180.

[33] Gara F, Nicoletti V, Carbonari S, Ragni L, Dall'Asta A. Dynamic monitoring of bridges during static load tests: influence of the dynamics of trucks on the modal parameters of the bridge. J Civ Struct Health Monit Apr. 2020;vol. 10(2):197–217. https://doi.org/10.1007/s13349-019-00376-1.

[34] Yang YB, et al. A novel frequency-free movable test vehicle for retrieving modal parameters of bridges: Theory and experiment. Mech Syst Signal Process May 2022;vol. 170:108854. https://doi.org/10.1016/j.ymssp.2022.108854.

[35] Chang KC, Kim CW, Borjigin S. Variability in bridge frequency induced by a parked vehicle. Smart Struct Syst May 2014;vol. 13(5):755–73. https://doi.org/10.12989/SSS.2014.13.5.755.

[36] S. Wei, 'Output only modal analysis -Scaled mode shape by adding small masses on the structure'.

[37] 'Ponts en acier (TGC volume 12) - Conception et dimensionnement des ponts métalliques et mixtes acier-béton - Jean-Paul Lebet, Manfred A. Hirt (EAN13: 9782880747657)', EPFL Press. Accessed: Nov. 02, 2023. [Online]. Available: https://www.epflpress.org/produit/63/9782880747657/ponts-en-acier-tgc-volume-12

[38] R.J. Allemang and D.L. Brown, 'A Correlation Coefficient for Modal Vector Analysis', presented at the Proceedings of the 1st International Modal Analysis Conference (IMAC I), Orlando, Nov. 1982, pp. 110–116.